

Atomic Layer Deposition of Metal phosphates

Lowie Henderick, Arpan Dhara, Andreas Werbrouck, Jolien Dendooven, and
Christophe Detavernier*

Department of solid state sciences, Ghent University, Krijgslaan 281 S1, 9000 Gent, BE

E-mail: christophe.detavernier@ugent.be

Abstract

Because of their unique structural, chemical, optical and biological properties, metal phosphate coatings are highly versatile for various applications. Thermodynamically facile and favorable functionalization of phosphate moieties (like orthophosphates, metaphosphates, pyrophosphates, phosphorus-doped oxides...) make them highly sought-after functional materials as well. Being a sequential self-limiting technique, atomic layer deposition has been used for producing high quality conformal coatings with sub-nanometer control. In this review, different atomic layer deposition based strategies used for the deposition of phosphate materials are discussed. The mechanisms underlying those strategies are discussed, highlighting advantages and limitations of specific process chemistries. In a second part, the application of metal phosphates deposited through atomic layer deposition in energy storage and other emerging technologies such as electrocatalysis, biomedical or luminescence applications are summarized. Next to this, perspectives on untangled knowledge gaps and opportunities for future research are also emphasized.

Introduction

Atomic Layer Deposition (ALD) has proven to be a successful thin film deposition technique providing reproducible stoichiometry, atomic-level thickness control and excellent conformality.¹ In this technique, a sample is exposed to a number of cycles, consisting of sequential pulses of different gaseous precursors. Each of those reacts with the substrate in a self-limiting manner. It is this self-limitation that distinguishes ALD from the more common Chemical Vapour Deposition (CVD) technique, in which the substrate is also exposed to one (or more) gaseous precursors. Conformal coatings on complex surfaces are harder to attain with CVD. As this self-limitation allows for depositing the same minute amount of material in each ALD deposition cycle, the thickness of ALD-deposited films can be tailored to sub-nanometer level.

Due to these interesting properties, a lot of work has been done over the last years to extend the number of different materials that can be deposited using ALD.² Metal oxides such as Al_2O_3 ,³ ZnO ⁴ and TiO_2 ⁵ are by far the most studied class of materials followed by metals,⁶ fluorides⁷ and sulfides.⁸ Extensive effort on ALD of phosphates only started recently, as the search for an appropriate phosphorus precursors proved to be quite difficult. In the ongoing search for suitable ways to create phosphorus-containing layers, more and more successful depositions of different types of metal phosphates are being reported. A review on ALD of this specific class of materials is, however, at this time not yet present.

The interest in phosphate materials mainly comes from the strong covalent P-O bonds which arise from the hybridisation with the phosphorous *d*-orbital within the phosphate moiety.^{9,10} Most of the naturally obtained P-containing materials are phosphates which implies the chemical and structural stability of this polymorph. Owing to their wide range of physico-chemical properties, the applications of phosphates are multi-fold. Although the majority of work on ALD of phosphates so far in literature has been aimed towards their implementation in Li-ion batteries, their possibilities are not restricted to these applications only. In term of thin film applications, phosphate coatings are commercially popular as a

This is the author's peer reviewed, accepted manuscript. However, the online version of record will be different from this version once it has been copyedited and typeset.

PLEASE CITE THIS ARTICLE AS DOI: 10.1063/1.50069647

protection layer on metal parts for corrosion resistance and lubrication.¹¹ The phosphate framework can also increase the emission in luminescent materials,¹² improve reinforcement properties in composites,¹³ etc. When focusing on energy storage, the P-O framework can offer a lot of advantages for its use as an electrode or coating in both Li-ion batteries (LIB) and Na-ion batteries (SIB). Long-term structural and thermal stability, and low volume expansion of these frameworks upon charging and discharging are beneficial in extending cycling life of the battery electrodes.^{14,15} Additionally, the use of phosphates as a battery electrode is advantageous over metal oxides when it comes to its potential with respect to Li^+/Li , due to the inductive effect of the polyanions.¹⁶ Transition metal phosphates are also widely explored as oxygen evolution catalysts in alkaline and neutral media, which can find application in renewable energy conversion and storage systems.¹⁷ In these systems, the phosphate anion can act as a proton acceptor to facilitate oxidation of the metal atom and the local metal geometry can be adjusted to optimise water absorption and oxidation, making the transition metal phosphates promising catalysts for the Oxygen Evolution Reaction (OER).

In this review, a recapitulation will be made on the different aspects of the deposition of phosphates through ALD. Different precursors that can be used for the deposition of phosphorus containing films will be discussed, as well as the mechanisms underlying the deposition process. Next to this, the effect of ALD process parameters on (amorphous) phosphate structures will be treated. Finally, the applications of ALD-deposited phosphate thin-films within different research fields will be summarized with a focus on Li-ion batteries and electrocatalysis.

Phosphate characterisation

Prior to discussing the deposition of phosphates using ALD, a brief explanation on general phosphate classification will be presented as well as how a phosphate can be structurally characterised. Such an understanding is key in order to achieve optimal practical implementation of present and future phosphate ALD processes. In the following a phosphate will be defined as a material consisting of P and O atoms, and possibly one or more additional metal species. In this compound, the phosphorus atom has valence 5, and it is surrounded with 4 oxygen atoms, of which one is doubly bonded to the phosphorus atom.

General phosphate classifications

Usually phosphates are classified along their network forming properties. If every O atom connects two P atoms, the network is called a polyphosphate, and consists of $\text{PO}_{2.5}$ building blocks (equivalent to fully connected PO_4 blocks with 3 O atoms shared between PO_4 units). Some metal atoms with valence ν might come in at the expense of more O atoms, until a structure called metaphosphate is reached: P atom has on average one doubly bond O, two O's binding to other P atoms and one metal atom. Still, the backbone of the structure is the P-O-P structure. When further increasing the metal content, a transition is made to pyrophosphates and finally to orthophosphates. Now every PO_4 unit is fully disconnected from other PO_4 units. The metal atoms bridge between the PO_4 units. If we go further and add even more metal, the backbone of the material becomes the metal oxide, with ever less phosphorus doping. It is important to realize that the O/P content increases along with the metal content of the material. As the oxygen content grows consistently with the metal content, the O/P ratio is a decent way to gauge the connectedness of phosphate networks. The lower the O/P ratio, the more connected the phosphate network is. This metric allows easy comparison of depositions of different materials under similar conditions and with similar precursors. The last paragraph can be summarized by the following equation:

This is the author's peer reviewed, accepted manuscript. However, the online version of record will be different from this version once it has been copyedited and typeset.

PLEASE CITE THIS ARTICLE AS DOI: 10.1063/1.50069647

$$[O] = 2.5[P] + 0.5\nu[M] \quad (1)$$

where the H and C concentration are not captured in this equation and are hence a source of error. However these elements are seldom reported, either because (a) they are not present in the film (b) the used techniques are not able to detect these species (c) no clear reason. Where they are reported, the concentrations of these species are typically low, below 10% of the film. Note that the presented relationship still holds when the phosphorus content goes to 0. The relationship between O/P, M/P and M/O ratio that follows from equation 1 can be seen from Fig. 1. From this figure, it can be inferred that the more often reported P/M ratio contains similar information, but mediated by the valence ν of the atom. As this ratio

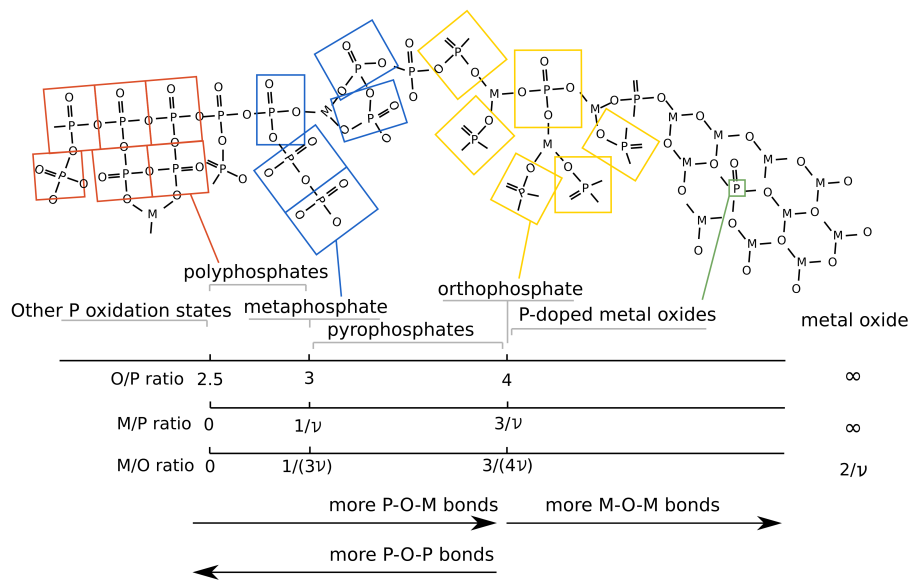


Figure 1: Different phosphate stoichiometries. In certain compositions, dependent on the metal, a crystalline phase may be energetically favorable. However, most ALD-deposited materials will be in the amorphous phase. Some O atoms at the edges of the network are omitted for clarity. The M/P and M/O ratios are mainly dependent on the valence ν of the metal.

is reported more often, it will be used as an indication of how well the phosphorus precursor in question allows for the deposition of the targeted metal phosphate-like material. It does need to be noted that the stoichiometry does not tell the full story on the material chemistry. A change in for example the P/M ratio does not necessarily provide information on how the phosphate structure (i.e. how every element is exactly incorporated in the material) itself changes. For this, a more detailed characterisation would be needed as will be explained in the following section. However, as such a detailed characterisation is often missing in the ALD of phosphates literature, the stoichiometry will still be used here to get an initial idea on the process and layer chemistries.

For a deeper structural understanding of phosphates, we refer the interested reader to the paper of Brow *et al.*¹⁸

Material characterization

In most cases, the phosphates that can be deposited using ALD are amorphous as-deposited. The deposited material can be crystallised in some cases using a post-deposition anneal, but this is not always preferred. Due to the amorphous nature of the as-deposited material, the characterisation techniques are limited. In this subsection, the possible ways to extract structural information on the material of interest will be discussed.

A general compositional characterization of phosphates can be achieved with EDX, XPS, ERD, RBS, and so on. However, reports on phosphate ALD pay, in general, little attention to the underlying structure of the deposited material. All too often, as soon as the material contains some phosphorus, it is classified under the passe-partout phosphate denominator. A main reason of the difficulty in classifying these amorphous materials is that their stoichiometry and properties span a continuum rather than the discrete classes and distinct phases of their crystalline counterparts (figure 1). Using the classification from the previous section we can conclude that from compositional information alone, even if incomplete, some structural information can already be inferred. The previously introduced connectedness of

the PO_4 group could be used to classify the amorphous systems in more detail, as material properties obviously depend not only on the overall composition, but as well on how the groups are interlinked. We are aware that using compositional data to conclude something about amorphous structure is prone to over-interpretation, but for the lack of better ways of comparing the reported materials this is exactly what we will do in this review.

A second manner of structurally characterizing phosphates is offered by infrared spectroscopy. These techniques can be used in situ to probe the surface groups, but those are as well sensitive to the structure of the deposited *bulk* material.^{19,20} Different parts from the network have different signatures in infrared spectra, and Raman and FTIR measurements offer complementary information here. While difference spectra from in situ measurements, as for example performed in the work of Dobbelaere et al.²¹ can be very instructive to gain insight in the reaction process, we find that often IR measurements of the bulk films can be as interesting.

Identification of the peaks can be daunting, though. We refer to the standard reference works of Socrates²² and Nakamoto²³ to enable interpretation of peaks. Based on these works, the regions where phosphate related peaks can be found are visualised in figure 2(a). Next to this, an ex-situ FTIR spectrum of an ALD deposited Al phosphate is shown (figure 2(b)) to give an idea of what a typical spectrum could look like with varying phosphorus content. In studying such a spectrum, the relative intensity of the P=O, P-O-P and M-O peaks could essentially also be informative to get structural insight. These trends are indicated at the bottom of fig. 1. However, in this review the FTIR measurements will only be briefly discussed and serve more as an indication of phosphate type growth and a tool for process characterisation rather than for gaining structural insights.

We also want to point the reader towards the interesting work of Popovic et al. on the correlation between Raman wavenumber of the PO bond, and its length, in all different kinds of phosphates: an empirical relationship between those properties was obtained.²⁰

Another characterisation technique, NMR (often used for glass characterization), has

This is the author's peer reviewed, accepted manuscript. However, the online version of record will be different from this version once it has been copyedited and typeset.

PLEASE CITE THIS ARTICLE AS DOI: 10.1063/1.50069647

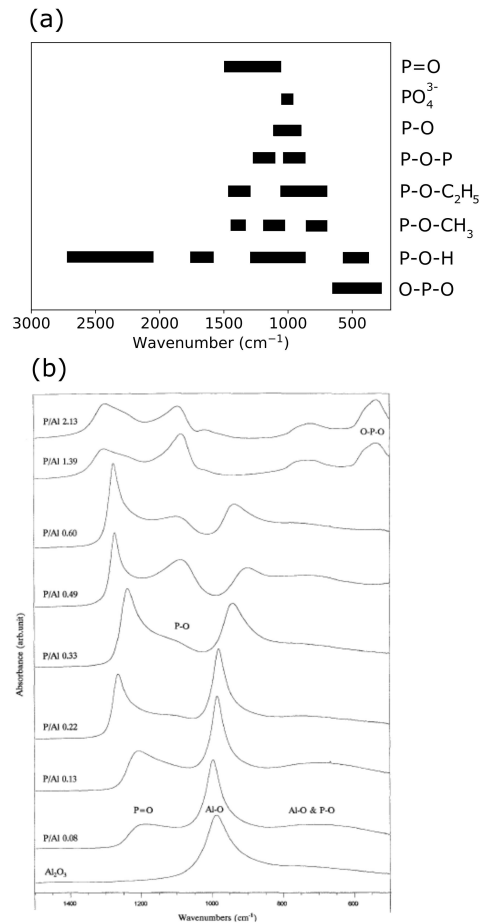


Figure 2: (a) Visualisation of a selection of relevant IR frequencies. For more detailed peak positions we refer to²² and.²³ (b) Example of FTIR spectra resulting from ALD of aluminum phosphate with a varying P/Al ratio in the work of Nieminen et al.,²⁴ showing the formation of a phosphate at high P/Al ratios. Reprinted with permission from [24]. Copyright 1995 Springer.

limited sensitivity towards thin-film materials. Hence it is rarely used to investigate ALD films²⁵ but it is a staple technique in glass science. Synchrotron-based techniques such as

HE-XRD²⁶ are less common, but suitable to determine for example the pair distribution function (PDF) or the distribution of interatomic distances.

ALD of phosphates

With this knowledge on the material characterisation in mind, the deposition of phosphates using ALD can be discussed in more detail. First of all, the different kinds of phosphorus precursors that could allow for phosphate deposition will be discussed. After this, the growth per cycle will be defined as an important ALD process characteristic, allowing for a complete overview of the currently available ALD phosphate processes. Finally, an additional analysis on the connectedness of various reported materials will be presented as well as a discussion on the various ALD reaction mechanisms.

Phosphorus-containing precursors

The first step in trying to enable the growth of a phosphate through ALD is finding a precursor suitable for the incorporation of the phosphate anion. In general, the ALD precursors should essentially fulfill two major criteria: i) good volatility and thermal stability and ii) high reactivity towards various surface species at the substrate surface. Non-metal precursors are ideally hydrides (like H_2O for oxide, H_2S for sulfide, NH_3 for nitride, AsH_3 for arsenide *etc.*) having excellent volatility and thermal stability along with high reactivity. Likewise, one can predict phosphoric acid H_3PO_4 to be the ideal hydride analogue for phosphate building blocks. However, H_3PO_4 is not volatile at room temperature and polymerizes into various polyphosphoric acid forms upon heating by releasing water vapour. Thus, alternative approaches and chemistries are essential to enable phosphate ALD.

It is interesting to consider that phosphates are amongst the first materials developed in the 60's era, produced from P_2O_5 monolayers.²⁷ The formation of a P_2O_5 layer was achieved by sequential exposure of PCl_3 and H_2O . Halide precursors like PCl_3 used to be very popular

in earlier days because they satisfy the two aforementioned criteria very well. However, due to the high deposition temperature and corrosive/toxic by-products created during the ALD made, these precursors are not often used any more. Eventually, two articles in the late 90's presented P_2O_5 as an alternative phosphorous precursor. In spite of being a simple, cheap and less toxic compound compared to PCl_3 , the high temperature requirement (in the range of 170-350°C) in order to achieve considerable vapour pressure makes P_2O_5 less practical to use as ALD precursor.

In recent years, the most widely used precursor for phosphate ALD is trimethyl phosphate (TMP). The high volatility, stability, low cost and considerably reduced toxicity makes TMP an outstanding ALD precursor. Most of the metal phosphate ALD reported in the literature which include Al, Ti, Ca, Li, La, Fe, Eu-Ti, Li-Fe has been produced using TMP as the source of the phosphate building block. Knohl et al. used an ethyl substituted version (triethyl phosphate, TEP) to develop $AlPO_4$ films. An amine substituted version diethyl phosphoramidate (DEPA) has been used to incorporate nitrogen into the deposited films. Shibata et al. used tris-dimethylaminophosphorus (TDMAP) in combination with NH_3 as the precursors to produce nitrogen-incorporated phosphate films.²⁸ The phosphorous precursors reported that have allowed for the deposition of phosphates in literature are represented in figure 3, along with their chemical structure, physical state at room temperature and vapour pressure at given temperature.

Despite of being a regular choice of precursor, the main limitation associated with TMP is the low reactivity of terminal $-OCH_3$ groups towards most metal-organic compounds and hydroxyl groups. To resolve this issue, TMP is typically either combined with a halide co-reactant²⁹ or with ozone/oxygen-plasma to remove $-CH_3$ groups.^{30,31} More recently, Dobbe-laere et al. presented a plasma-based approach to solve the reactivity issue,²¹ as will be discussed in detail in the following sections.

Other phosphorus containing precursors have been reported as well, but these have not been investigated for the deposition of phosphates in particular. The use of PH_3 has for example

already allowed for the deposition of GaP,³² where the addition of an oxygen containing gas in the ALD process might allow for a phosphate structure to be formed. However, more research would be needed to verify this suitability towards the deposition of phosphates. For a more extensive overview of all reported phosphorus containing precursors (i.e. not only the ones used in ALD of phosphates literature) we refer to the review article of Miikulainen et al.²

Growth per cycle

An important measure to characterise an ALD process is the GPC (growth per cycle), which is the increase in thickness after the completion of one full ALD cycle. As ALD processes for phosphates often involve metal- as well as phosphorus-type subcycles (as will be discussed in more detail later), the total length of the ALD process can also be taken into account by dividing the growth per cycle (listed in table 1) by the total amount of subcycles (metal-based sub-cycles plus phosphorus-based sub-cycles). This metric is defined here as the growth-per-sub-cycle ratio, giving a more realistic (and normalised) idea of the deposition speed of the metal phosphate under discussion. The growth and final thickness of the films are typically measured with techniques such as XRR or (spectroscopic) ellipsometry.

Metal phosphate ALD processes

Table 1 summarises the different ALD processes that have been proposed for the deposition of metal phosphates, as well as some important metrics to characterise the growth. The table lists the reactants and co-reactants, as well as the amount of metal-based sub-cycles with respect to phosphorus-based sub-cycles. A visualisation of the growth-per-subcycles and P/M ratios (the available O/P ratios will be discussed separately) obtained from this table is presented in figure 4. Using this overview, the currently available processes for ALD of metal phosphates can be discussed in more detail.

This is the author's peer reviewed, accepted manuscript. However, the online version of record will be different from this version once it has been copyedited and typeset.

PLEASE CITE THIS ARTICLE AS DOI: 10.1063/1.50069647

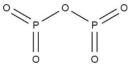
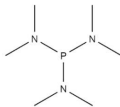
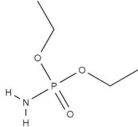
	Chemical representation	Physical state at room temperature	Vapour pressure at specific temperature
Trimethylphosphate (TMP)		Liquid	1.3 mbar @ 25°C
Phosphorus trichloride (PCl ₃)		Liquid	160 mbar @ 25°C
Diphosphorus pentoxide (P ₂ O ₅)		Solid	0.02 mbar @ 250°C
Triethylphosphate (TEP)		Liquid	0.5 mbar @ 25 °C
Tris(dimethylamino)-phosphorus oxide (TDMAP)		Liquid	0.09 mbar @ 25°C
Diethylphosphoramidate (DEPA)		Solid	0.09 mbar @ 25°C
Phosphoryl chloride (POCl ₃)		Liquid	53 mbar @ 27°C

Figure 3: List of precursors that have been reported in the ALD of phosphates literature, including their physical state and vapour pressure.

This is the author's peer reviewed, accepted manuscript. However, the online version of record will be different from this version once it has been copyedited and typeset.

PLEASE CITE THIS ARTICLE AS DOI: 10.1063/5.0069647

Table 1: Overview of ALD processes depositing phosphorus-containing materials, an asterisk (*) denotes plasma enhanced ALD. If both substrate temperature and P:M cycle ratio were varied in the reported work, superscripts T (temperature) and C (cycle ratio) were used to denote which parameter affected the growth per cycle and P:M atomic ratio. If the reported measurements were performed at a specific value in the temperature/cycle ratio space (for example varying the cycle ratio at one specific substrate temperature instead of the whole temperature window), the value is also specified in the superscript. For more detailed information, the reader is referred to the manuscript in question.

Element	Metal source	Coreactant	P source	Coreactant	T_{sub} (°C)	GPC (nm)	P:M cycle ratio	P:M atomic ratio	Ref.	
Aluminum	AlCl ₃	H ₂ O	P ₂ O ₅	/	500	N.A.	1:60 – 1:5	0.18 – 1.28	1995 ²⁴	
	AlCl ₃	/	TMP	H ₂ O	500	N.A.	1:60 – 1:5	0.06 – 0.37	1995 ²⁴	
	AlCl ₃	H ₂ O	P ₂ O ₅	H ₂ O	500	0.13 ^{1:5}	1:5 – 1:30	1.02 – 0.25	1998 ³³	
	AlCl ₃	C ₄ H ₉ OH	P ₂ O ₅	C ₄ H ₉ OH	500	0.11 ^{1:5}	1:5 – 1:20	1.41 – 0.04	1998 ³³	
	AlCl ₃	/	TMP	/	150 – 400	0.14 – 0.24	1:1	0.4 – 0.6	2012 ²⁹	
	TMA	H ₂ O	TMP	O ₃	150	1.7 ^{20:1}	5:1 – 20:1	0.2 – 0.8	2013 ³¹	
	TMA	H ₂ O	TMP	H ₂ O	250	N.A.	1:1	N.A.	2017 ³⁴	
	TMA	/	TEP	/	250	0.14	1:1	0.2 – 0.3	2013 ³⁵	
	TMA	O ₂ *	TMP	O ₂ *	25 – 300	0.18 ^{150,C} – 0.46 ^{150,C}	1:1 – 10:1	0.5 ^{150,C} – 1.4 ^{150,C}	2020 ³⁶	
	TMA	/	TMP*	O ₂ *	320	0.37	1:1	1.8	2014 ²¹	
	(N doped)	TMA	/	DEPA*	N ₂ *	325	1.4	1:1	3.6	2020 ³⁷
	TMA	/	DEPA*	O ₂ *	325	0.6	1:1	2.2	2020 ³⁷	
	Chromium	CrO ₂ Cl ₂	H ₂ O	PCl ₃	H ₂ O	180	N.A.	N.A.	N.A.	1969 ²⁷
Boron	TMB	/	POCl ₃	/	600	N.A.	N.A.	N.A.	1993 ³⁸	
Calcium	Ca(thd) ₂	O ₃	TMP	H ₂ O	275 – 300	0.041 ^{11:1,T}	1:3 – 11:1 (approx.)	0.1 ^C – 1 ^C (approx.)	2009 ³⁹	
	Ca(thd) ₂	O ₃	TMP	H ₂ O	300	0.24	1:6	0.6	2013 ⁴⁰	
Tin	TDMASn	/	TMP	H ₂ O + O ₃	225 – 250	0.12 – 0.18	1:1	0.11 – 0.17	2015 ⁴¹	
Lithium	LiHMDS	/	TMP	/	275 – 350	0.04 – 0.13	1:1	0.34 – 0.36	2012 ⁴²	
	LiO ^t Bu	/	TMP	/	225 – 300	0.07 – 0.1	1:1	0.36 – 0.38	2012 ⁴²	
	LiO ^t Bu	/	TMP	/	275 – 325	0.057 – 0.072	1:1	0.30 – 0.36	2014 ⁴³	
	LiO ^t Bu	/	TMP	/	250 – 300	0.042 – 0.06	1:1	N.A.	2016 ⁴⁴	
	LiHMDS	/	TMP	/	325	0.08	1:1	0.38	2020 ⁴⁵	
	(hybrid coating)	LiO ^t Bu or TTIP	/ or H ₂ O	TMP or /	/	250	0.087	1:1 + 2 cycles TiO ₂	N.A.	2016,2019 ^{46,47}
	(LiPON)	LiO ^t Bu	H ₂ O	TMP	N ₂ *	150 – 250	0.070 – 0.105	1:1	0.36 – 1.3	2015, 2017 ^{48,49}
	(LiPON)	LiO ^t Bu	H ₂ O	TMP	N ₂ *	250	0.105	1:1	N.A.	2016 ⁵⁰
		LiO ^t Bu	H ₂ O	TMP	\	200 – 275	N.A.	1:1	0.31 – 0.42	2019 ⁵¹
	(LiPON)	LiO ^t Bu	H ₂ O	TMP	N ₂ *	200 – 275	N.A.	1:1	0.55 – 0.53	2019 ⁵¹
	(LiPON)	LiHMDS	N ₂	DEPA	N ₂	270 – 310	0.06	1:1	1.11 – 1.05	2015 ⁵²
	(LiPON)	LiO ^t Bu	\	DEPA	\	250 – 300	0.065 – 0.095	1:1	0.59 – 0.53	2017 ⁵³
	(LiPON)	LiO ^t Bu	NH ₃	TDMAP	O ₂	400 – 500	0.21 ⁴⁵⁰	1:1	0.43 ⁴⁵⁰	2016 ²⁸
Titanium	TiCl ₄	H ₂ O	PCl ₃	H ₂ O	180	N.A.	N.A.	N.A.	1969 ²⁷	

This is the author's peer reviewed, accepted manuscript. However, the online version of record will be different from this version once it has been copyedited and typeset.

PLEASE CITE THIS ARTICLE AS DOI: 10.1063/5.0069647

Table 1 continued from previous page

Element	Metal source	coreactant	P source	Coreactant	T _{sub} (°C)	GPC (nm)	P:M cycle ratio	P:M atomic ratio	Ref.
(N doped)	TiCl ₄	H ₂ O	TMP	H ₂ O	150 - 300	0.12 ²⁵⁰	1:1	0.90 - 1.70	2012 ³⁰
	TiCl ₄	/	TMP	/	275 - 450	0.14 ³⁵⁰	1:1	1.25 - 1.66	2012 ⁴⁹
	TiCl ₄	/	TEP	/	200	0.22	1:1	0.33	2018 ¹³
	TTIP	/	TMP*	O ₂ *	300	0.66	1:1	1.7	2017 ⁵⁴
	TTIP	/	DEPA*	N ₂ *	300	0.6	1:1	3.3	2021 ⁵⁵
	TTIP	/	DEPA*	O ₂ *	300	0.7	1:1	2.5	2021 ⁵⁵
Iron	Fe(Cp) ₂	O ₃	TMP	H ₂ O	200 - 350	0.02 - 0.06	1:1	1.25 - 0.77	2014 ⁵⁶
	(LiFePO ₄)	Fe(Cp) ₂ /LiO ^t Bu	O ₃ /H ₂ O	TMP	H ₂ O	300	0.94	1:1	1.1
(LiFePO ₄)	Fe(Cp) ₂	O ₃	TMP	H ₂ O	300	0.06	1:1	1.25 - 0.77	2015 ⁵⁷
	FeCl ₂ / LiO ^t Bu	H ₂ O / H ₂ O	TMP	H ₂ O	300	N.A.	1:1	0.19 - 0.31	2019 ⁵⁸
	Fe(thd) ₃	O ₃	TMP	H ₂ O+O ₃	246 - 360	0.03 ^{1:1,T}	1:1, 1:4, 2:3	N.A.	2013 ⁵⁹
	Fe(thd) ₃	O ₃	TMP	H ₂ O+O ₃	250	0.18 - 0.1	2:3, 1:2, 1:3, 1:4	1.5 - 0.75	2020 ⁶⁰
	TBF	/	TMP*	O ₂ *	300	1.1	1:1	1.5	2016 ⁶¹
Lanthanum	La(thd) ₃	O ₃	TMP	H ₂ O+O ₃	250 - 300	0.08 ^{1:1,T}	0:1 - 3:1	0.00 ^C - 1.00 ^C	2014 ⁶²
Zinc	DEZ + TMP	O ₃	/	/	250	0.17	N.A.	N.A.	2011 ⁶³
	DEZ	H ₂ O	TMP	H ₂ O	160	0.19 - 0.16	N.A.	N.A.	2012 ⁶⁴
	DEZ	/	TMP*	O ₂ *	300	0.92	1:1	2.2	2016 ⁶⁵
Cobalt	Co(Cp) ₂	O ₂ *	TMP	O ₂ *	100 - 300	0.13 ^{1:1,T} - 0.11 ^{1:1,T}	1:1, 11:12	0.62 ^{300,C} - 0.53 ^{300,C}	2019, 2020 ^{66,67}
	Co(Cp) ₂	/	TMP*	O ₂ *	300	0.8	1:1	2.3	2019 ⁶⁸
Vanadium	TEMAV	/	TMP*	O ₂ *	300	0.78	1:1	0.88	2017 ⁶⁹
Magnesium	Mg(EtCp) ₂	H ₂ O	TDMAP	O ₂ *	125 - 300	0.14 - 0.12	1:1	0.82 - 0.67	2019 ¹⁹
Sodium	NaO ^t Bu	/	DEPA	/	300 - 400	0.01 - 0.1	1:1	1	2020 ⁷⁰
POx	/	/	TMP	O ₂ *	25	0.11	N.A.	N.A.	2017 ⁷¹
	/	/	TMP ⁱ	O ₂	150-450	N.A.	1:1	N.A.	2020 ⁷²
(SiO _x intermixed)	(Si(NMe ₂) ₃)	(O ₂ *)	HMPT(/TEP)	O ₂ *	150 - 200	N.A.	N.A.	N.A.	2018 ⁷³

14

1

¹Some chemical compounds were labelled with an abbreviation. Their full names are listed here. Trimethyl phosphate (TMP), trimethylaluminum (TMA), triethyl phosphate (TEP), diethyl phosphoramidate (DEPA), trimethyl borate (TMB), titanium isopropoxide (TTIP), tert-butylferrocene (TBF), diethyl zinc (DEZ), tetrakis(ethylmethylamido) vanadium (TEMAV), tris-dimethylaminophosphorus (TDMAP), hexamethylphosphorous triamide (HMPT) trimethyl phosphite (TMPⁱ)

This is the author's peer reviewed, accepted manuscript. However, the online version of record will be different from this version once it has been copyedited and typeset.

PLEASE CITE THIS ARTICLE AS DOI: 10.1063/1.50069647

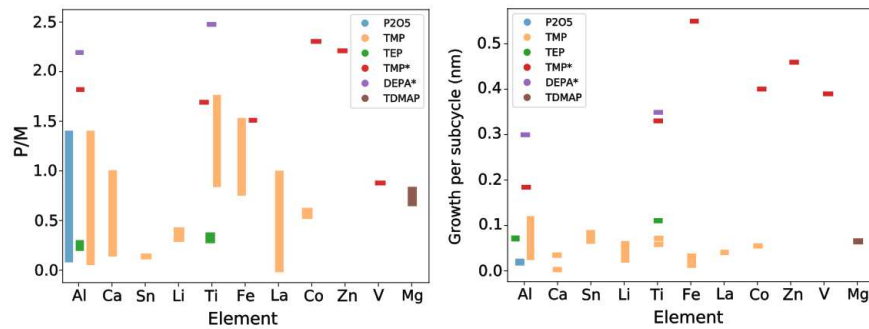


Figure 4: Visualisation of two important parameters obtained from table 1 with (left) an overview of the reported P/M values and (right) growth per subcycles (growth per cycle divided by the total amount of subcycles) of the un-doped metal phosphates.

Early metal phosphates ALD. The first phosphate-related ALD-like processes were reported already in 1969 by Kol'tsov et al.²⁷ In this work, monolayers of PO_x could be formed by sequential exposure of PCl_3 and water. Deposition of titanium phosphate became possible by mixing these monolayers with TiO_2 monolayers. This approach could be extended towards the deposition of chromium phosphate,⁷⁴ by combining the PO_x layers with chromium oxide. Although PCl_3 was never used again in later research towards ALD of phosphates, this seminal work introduced the intermixing of phosphorus containing sublayers with metal oxides to achieve the deposition of the targeted metal phosphate. The introduction of such a sub-cycle approach for the deposition of a phosphate is a clear indication of how complex these processes can become with respect to the more standard two-step approach of typical metal-oxides. An illustration of the two different approaches that can be followed for the deposition of an ALD metal phosphate is shown in figure 5, where (a) describes the standard sub-cycle approach with two clearly separated oxide cycles and (b) a more standard two- (only the metal and phosphorus precursor are pulsed) or three-step (using an additional co-reactant after one of both precursors) process that in some cases can also allow for ALD of a metal phosphate.

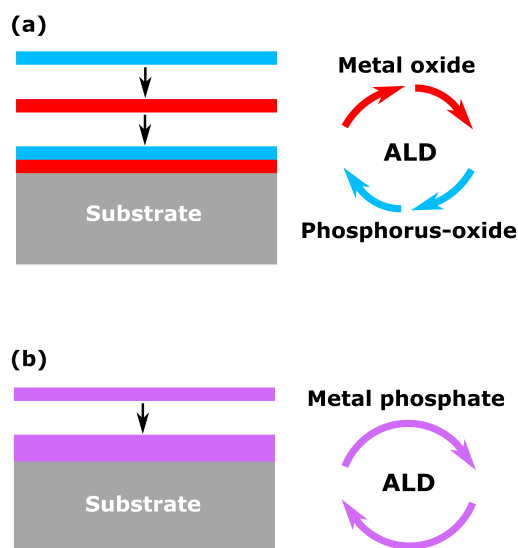


Figure 5: Visualisation of two deposition paths that can be followed for ALD of a metal phosphate. Each coloured block implies monolayer growth by a complete (sub-)cycle containing two or more precursors (with a precursor and/or reactant pulse indicated by a coloured arrow). (a) One ALD cycle consists of clearly separated metal-oxide and phosphorus oxide steps. (b) A more typical two- (or three-) step process involving direct reactions between the metal and phosphorus precursor (or with potentially one additional co-reactant step).

Two decades later (1995), the sub-cycle approach was also followed by Nieminen et al.²⁴ for the deposition of aluminium phosphate using P_2O_5 as the phosphorus-containing precursor. It was found that, instead of using PCl_3 and water to form a PO_x monolayer, adding a cycle of P_2O_5 (i.e. $AlCl_3 - H_2O - P_2O_5$) or trimethylphosphate and water (i.e. $AlCl_3 - TMP - H_2O$) after every few aluminium oxide cycles allowed for phosphorus incorporation into Al_2O_3 . Although the sub-cycle approach can be quite lengthy and complex, it does offer the benefit that by changing the amount of phosphorus oxide to aluminium oxide cycles, the phosphorus content in the layer could be controlled. When the concentration exceeded 5 at.%, phosphorus diffused into the Al_2O_3 layer to form aluminium phosphate. The formation of a phosphate structure was evidenced by the FTIR spectrum presented earlier in figure

This is the author's peer reviewed, accepted manuscript. However, the online version of record will be different from this version once it has been copyedited and typeset.

PLEASE CITE THIS ARTICLE AS DOI: 10.1063/1.50069647

2(b), where the peaks attributed to Al_2O_3 tend to disappear at higher P/Al weight-ratios (closer to the stoichiometric value for Al phosphate), while phosphate related bonds start to appear. Including more phosphorus oxide cycles per metal oxide cycle thus seems to lead to a shift from a phosphorus doped metal oxide towards a real phosphate phase. Looking at the phosphorus content of aluminium phosphate deposited using P_2O_5 or TMP, a much lower P/Al atomic ratio is found for the latter process. Therefore, comparatively more number of PO_x subcycles are required to reach a high P/Al atomic ratio. The substrate temperature in both processes was, however, 500°C , which is fairly high for typical ALD processes.

In a subsequent work, Tiita et al.³³ studied the mixing of Al_2O_3 layers (AlCl_3 in combination with water or 2-methyl-2-propanol as oxygen source) with phosphorus containing monolayers (i.e. $\text{AlCl}_3 - \text{H}_2\text{O}/2\text{-methyl-2-propanol} - \text{P}_2\text{O}_5 - \text{H}_2\text{O}/2\text{-methyl-2-propanol}$) at a substrate temperature of 500°C

. This process lead to the deposition of aluminium phosphate as evidenced by the presence of P-O bonds in the FTIR spectrum (figure 6(f)). A considerable decrease in phosphorous content and growth rate were observed when P_2O_5 was allowed to react right after AlCl_3 (i.e. without using a co-reactant), indicating that the P_2O_5 preferably reacts with an -OH terminated surface. The films deposited using 2-methyl-2-propanol as oxygen source (with a deposition rate of 0.11 nm/cycle), and P_2O_5 with 5:1 cycle ratio, were close to stoichiometric AlPO_4 and found to be crystalline with low impurities. By contrast, non-stoichiometric amorphous aluminium phosphate films with higher Cl contamination were produced using water as co-reactant.

Around the same time, boron phosphate was deposited by Brei et al.,³⁸ who combined trimethyl-borate (TMB) with POCl_3 . In this work, direct reactions between the adsorbed borate compound and the phosphorus precursor were proposed through the formation of B-O- PCL_2 surface groups, and CH_3Cl as a side product. However, the reported data is scarce (for example no reported growth rate and/or saturation), and the process was performed

This is the author's peer reviewed, accepted manuscript. However, the online version of record will be different from this version once it has been copyedited and typeset.

PLEASE CITE THIS ARTICLE AS DOI: 10.1063/1.50069647

at a substrate temperature of approximately 600°C, making it difficult to evaluate the true self-saturating behaviour of this process.

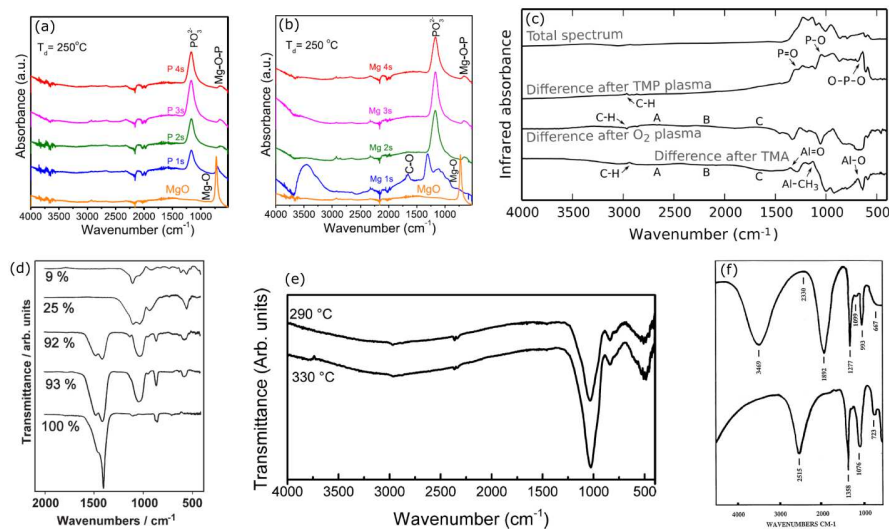


Figure 6: Different FTIR spectra used to confirm and further study the deposition of a phosphate-like material. (a,b) FTIR spectrum of magnesium phosphate in the work of Su et al.¹⁹ with respectively varying exposure of the phosphorus precursor and the metal precursor. (c) In-situ FTIR during the deposition of aluminum phosphate using a TMP* in the work of Dobbelaere et al.,²¹ unraveling the reaction mechanism. (d) FTIR spectra of the Ca-P-O thin films with varying Ca:P films from the work of Putkonen et al.³⁹ (e) FTIR spectra of thin film LiPON deposited at two different temperatures in the work of Nisula et al.⁵² (f) FTIR spectra during the deposition of phosphorus doped aluminum oxide using a 30:1 Al:P cycle ratio (top) and a 5:1 Al:P cycle ratio (bottom) in the work of Tiita et al. The source chemicals that are presented by each peak can be found in the work of Tiita et al.³³ Reprinted with permission from [19,21,33,39,52]. Copyright 2019 American Chemical Society, 2014 American Chemical Society, 2009 Elsevier, 2015 American Chemical Society, 1998 Elsevier.

In 2009, the research on ALD of phosphates continued with the seminal work of Putkonen et al.,³⁹ after which TMP became the most reported phosphorus source in the more recent ALD work. A new type of phosphate was introduced, calcium phosphate, based on the deposition

This is the author's peer reviewed, accepted manuscript. However, the online version of record will be different from this version once it has been copyedited and typeset.

PLEASE CITE THIS ARTICLE AS DOI: 10.1063/1.50069647

of calcium oxide ($\text{Ca}(\text{thd})_2 - \text{O}_3$). Combining this with a binary phosphorus oxide process (TMP – H_2O) at a substrate temperature between 275°C-300°C resulted in Ca-P-O layers at a deposition rate of 0.041 nm/cycle. Self-limited growth of the TMP precursor was observed, and the P/Ca atomic ratio could be varied by adjusting the amount of calcium oxide cycles with respect to phosphorus oxide cycles (similar to the sub-cycle technique introduced in earlier reports). By increasing the phosphorus content in the layer, the carbonates in the metal oxide framework showed to be replaced by phosphates (as seen in FTIR in figure 6(d)). This process was later (2013) also used by Ananda Sagari et al.,⁴⁰ where a decreasing P/Ca atomic ratio was found with increasing layer thickness. Adsorption of TMP molecules to the surface at initial growth was believed to have altered the atomic ratio. With increasing thickness, the ratio evolved towards 1.62, close to the stoichiometric value of 1.67 that was aimed for (by using a Ca:P cycle ratio of 6:1).

Deposition of lithium phosphates. After the work of Putkonen *et al.*, more and different types of phosphates were investigated. TMP could for example be used for the deposition of lithium phosphate, with either LiHMDS or LiO^tBu as metal precursor.⁴² These two precursors have proven to be the most volatile sources for lithium,⁷⁵ and showed good self-saturating behaviour in comparison with other lithium compounds. It is thus logical to investigate and compare these two precursors for the deposition of lithium containing phosphates. Lithium phosphate could be successfully deposited using the TMP – LiO^tBu process in a temperature window of 225°C-300°C (where the growth rate increased from 0.07 nm/cycle to 0.1 nm/cycle). It was found that, with increasing substrate temperature, carbon and hydrogen impurities decreased, suggesting more complete surface reactions at elevated temperatures. Deposition of lithium phosphate was also possible using TMP – LiHMDS, in a slightly higher temperature window of 275°C-350°C (where the growth rate increased from 0.04 nm/cycle to 0.13 nm/cycle). Near stoichiometric and crystalline Li_3PO_4 was obtained for both processes, although the latter contained a significantly higher amount of carbon (8.2

This is the author's peer reviewed, accepted manuscript. However, the online version of record will be different from this version once it has been copyedited and typeset.

PLEASE CITE THIS ARTICLE AS DOI: 10.1063/1.50069647

at.% vs. 2.7 at.%) and hydrogen (7.1 at.% vs. 5.1 at.%). Note that in both processes a direct reaction between the metal precursor and the phosphorus precursor is present, allowing for a basic two-step ALD process (figure 5(b)) to be implemented. Such a basic two-step process is not often reported in the field of phosphate ALD, but in some cases (such as the lithium phosphate) it does show to be possible. The reaction pathway in a LiHMDS-TMP process was further studied using mass spectrometry in the work of Werbrouck *et al.*,⁴⁵ and will be discussed later. It is interesting to note that effect of an oxygen plasma either after the TMP or after the LiHMDS pulse was also studied in this work, but in both cases the P/Li ratio decreased significantly while a significant amount of silicon was built into the film. Pulsing the oxygen plasma for example directly after the LiHMDS resulted in a P/Li ratio of 0.12, and pulsing it after the TMP resulted in a P/Li ratio of 0.20. The fact that a P/Li ratio of 0.38 can be obtained when no intermediate oxygen plasma is used, showed that this was the most optimal way of incorporating phosphorus in this case.

The successful deposition of lithium phosphate was later repeated in the work of Wang *et al.* (optimizing the ALD process for improved electrochemical results)⁴³ and Letiche *et al.* (for its use as a conformal solid electrolyte coating),⁴⁴ in which both combined TMP with LiO^tBu. In both deposition processes, the thermal activation of the process was seen in a temperature window of 275°C–325°C (Wang *et al.*) and 250°C–300°C (Letiche *et al.*). The growth rate was, however, slightly lower (respectively 0.057 – 0.072 nm/cycle and 0.042 – 0.06 nm/cycle) than in the work of Hamalainen *et al.* In the work of Wang *et al.*, this is thought to be related to the use of shorter pulse times for both precursors. The lower growth rate was not discussed in the work of Letiche *et al.* The work of Wang *et al.* was later also extended by trying to deposit a hybrid lithium phosphate - titanium dioxide layer (2 ALD cycles of TiO₂ per cycle of lithium phosphate) and using the resulting LTPO film either as a lithium ion battery electrode material⁴⁶ or as a thin coating layer on a high-voltage lithium ion battery electrode.⁴⁷

This is the author's peer reviewed, accepted manuscript. However, the online version of record will be different from this version once it has been copyedited and typeset.

PLEASE CITE THIS ARTICLE AS DOI: 10.1063/1.50069647

Lithium phosphorus oxynitrides (LiPON) are very promising materials in Li-ion battery applications, as the inclusion of nitrogen by breaking the P-O bonds can be promising in increasing the ionic conductivity of the phosphate glass. This motivated research on how the previous ALD processes for lithium phosphate could be altered to allow for nitrogen incorporation. Kozen et al.⁴⁸ reported ALD of LiPON using the TMP – LiO^tBu process as a starting point. First of all, it was found that including water exposure after LiO^tBu helps to complete the reactions (similar to an increase in substrate temperature), effectively decreasing the carbon contamination. Next, it was found that the addition of a nitrogen plasma exposure directly after the TMP exposure (i.e. TMP – N₂* - LiO^tBu – H₂O, where the star denotes a plasma) allowed for growth of nitrogen doped lithium phosphate at a rate of 0.105 nm/cycle. The substrate temperature in this work was 250°C although in later work it was shown that deposition at a temperature of 150°C is also possible (with a lower deposition rate of 0.07 nm/cycle).⁴⁹ It was also found that (at 250°C) changing the N₂*-dose allowed for altering the amount of nitrogen in the phosphate glass, without affecting the growth rate. As the amount of nitrogen can play a big role in the final electrochemical performance of the layer,⁷⁶ this tunability is very important. Put et al.⁵¹ found that at a fixed temperature, the nitrogen content could also be tuned by varying the power of the nitrogen plasma or the deposition temperature. As an increase in the plasma power allowed for a higher incorporation of triply coordinated nitrogen (one nitrogen bound to three phosphorus atoms, which is most efficient to reduce the number of O-P-O bonds in the final film), changing this parameter could allow for an efficient increase in the ionic conductivity of the phosphate glass.

Although this tunability is a significant advantage of the deposition process, the plasma step imposes an inherent limitation on the conformality. Thermal processes for depositing LiPON using TMP have, however, not been reported, which is thought to be related to the difficulty of cleaving the P-O bonds to create P-N bonds. Therefore, in a quest for thermal ALD of LiPON, Nisula et al.⁵² proposed diethyl phosphoramidate (DEPA) as an alternative phosphorus precursor. In combination with LiHMDS (which showed to be more stable in air

This is the author's peer reviewed, accepted manuscript. However, the online version of record will be different from this version once it has been copyedited and typeset.

PLEASE CITE THIS ARTICLE AS DOI: 10.1063/1.50069647

than LiO^tBu), thermal ALD of LiPON was demonstrated at a growth rate of 0.07 nm/cycle at a substrate temperature between 270°C–310°C. The composition of the film was measured to be $\text{Li}_{0.90}\text{PO}_{2.75}\text{N}_{0.55}$ and $\text{Li}_{0.95}\text{PO}_3\text{N}_{0.60}$ for the films deposited at 290°C and 330°C. The FTIR spectra of these films can be seen in figure 6(e) (mainly consisting of overlapping P-O and P-N vibrations).

In the work of Pearse et al.,⁵³ this approach was extended by changing the lithium precursor to LiO^tBu . The DEPA – LiO^tBu process showed an increasing growth rate from 0.015 nm/cycle to 0.09 nm/cycle when the substrate temperature was increased from 200°C to 300°C, which agrees with the before mentioned thermally activated growth of LiO^tBu . The use of LiO^tBu not only allowed for lower carbon content with respect to the process of Nisula et al. (similar to what is observed for undoped lithium phosphate), it also allowed for the deposition of a completely different class of ‘LiPON’ with composition closer to the $\text{Li}_2\text{PO}_2\text{N}$ stoichiometry ($\text{Li}_{1.7}\text{PO}_{2.1}\text{N}$ at 250°C and $\text{Li}_{1.9}\text{PO}_{2.1}\text{N}$ at 300°C) rather than a nitrogen substituted lithium metaphosphate (LiPO_3). This showed that the nature of the lithium precursor has a very important role in the reactions pathway during the ALD process. The report by Nisula et al. also provided growth monitoring with different precursor pulse times, proving that (at given conditions) DEPA can be used as a self-limiting phosphorus source. This data, along with an example for each of the other phosphorus precursors of which such measurements were available, is shown in figure 7(a).

Another thermal process for the deposition of LiPON was proposed in the work of Shibata et al.,²⁸ who combined trisdimethylaminophosphorus (TDMAP) with LiO^tBu and NH_3 (TDMAP – O_2 – LiO^tBu – NH_3). A nitrogen containing lithium phosphate ($\text{Li}_{2.35}\text{O}_{3.58}\text{PN}_{0.28}$) could be deposited, but growth was only reported well above what is typically considered as the thermal decomposition temperature of LiO^tBu ⁷⁷ (temperature window of the reported process was 400°C–500°C), putting in doubt the saturation behaviour of this process.

This is the author's peer reviewed, accepted manuscript. However, the online version of record will be different from this version once it has been copyedited and typeset.

PLEASE CITE THIS ARTICLE AS DOI: 10.1063/1.50069647

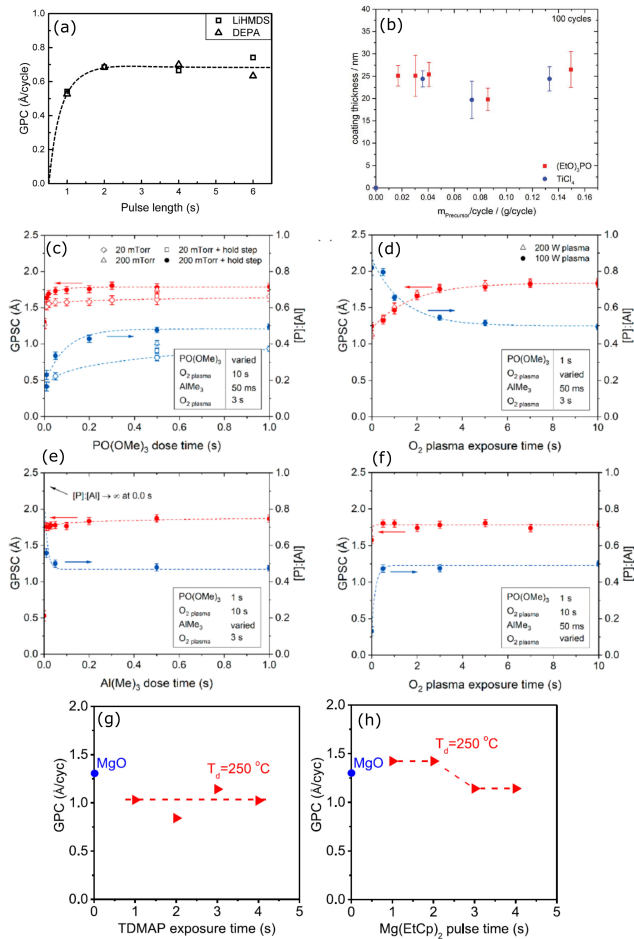


Figure 7: Saturated growth during the deposition of metal phosphates has been shown to be possible using different phosphorus precursors (similar data was not available for precursors other than the selection shown here). For each precursor, one example to prove saturation is shown with (a) the deposition of LiPON using DEPA - N_2 - LiHMDS - N_2 ,⁵² (b) deposition of titanium phosphate using TEP - $TiCl_4$,¹³ (c,d,e,f) deposition of aluminum phosphate using TMP - O_2^* - TMA - O_2^* ,³⁶ (g,h) the deposition of magnesium phosphate using TDMAP - O_2^* - $Mg(EtCp)_2$ - H_2O .¹⁹ Reprinted with permission from [13,52]. Copyright 2015 American Chemical Society, copyright 2018 Wiley. Reprinted with permission from <https://pubs.acs.org/doi/full/10.1021/acs.jpcc.0c00301> by [36]. Copyright 2020 American Chemical Society. Further permission related to the material excerpted should be directed to the ACS. Reprinted with permission from [19]. Copyright 2019 American Chemical Society.

This is the author's peer reviewed, accepted manuscript. However, the online version of record will be different from this version once it has been copyedited and typeset.

PLEASE CITE THIS ARTICLE AS DOI: 10.1063/1.50069647

Recent developments in metal phosphate ALD using chlorine based metal precursors. During the search for a good ALD process for LiPON, the deposition of other metal phosphates also further developed. In combining TMP with TiCl_4 , titanium phosphate was successfully deposited by Wiedmann et al.³⁰ Self-limiting growth at a substrate temperature between 200°C-250°C (with a growth rate of 0.12 nm/cycle and a stoichiometry of $\text{Ti}_3(\text{PO}_4)_4$) was, however, only found in the pulse sequence $\text{TMP} - \text{H}_2\text{O} - \text{TiCl}_4 - \text{H}_2\text{O}$, and not when one or two water pulses were omitted. The need for water pulses was explained by the presence of thermally unstable $\text{TiMe}_x\text{Cl}_{4-x}$ surface species without water pulses, and formation of more stable $\text{TiCl}_x(\text{OMe})_y$ species in the presence of water pulses.

In an attempt to simplify the deposition process, the growth of a metal phosphate without any co-reactants was revisited by Hämäläinen *et al.*,²⁹ similar to their work in lithium phosphate. Instead of working with sub-cycles to combine a metal oxide with a phosphorus oxide, a chlorine based metal precursor was directly combined with TMP. This was done for both aluminium phosphate ($\text{AlCl}_3 - \text{TMP}$) and titanium phosphate ($\text{TiCl}_4 - \text{TMP}$). In this way, the complexity of the deposition can be drastically reduced, but the accurate control of composition is sacrificed. For aluminium phosphate, growth of $\text{Al}_{2.6}\text{PO}_{7.0}$ and $\text{Al}_{1.6}\text{PO}_{5.6}$ was possible at respectively 200°C (growth rate of 0.15 nm/cycle) and 300°C (growth rate of 0.10 nm/cycle). This indicates that the fairly high substrate temperatures used in the work of Nieminen et al. are not necessary. Increasing the substrate temperatures reduced the chlorine and carbon content, showing incomplete reactions at these lower temperatures. For titanium phosphate, such a process was already attempted in the previously mentioned work of Wiedmann et al., in which the process without co-reactants did not show self-limiting growth. Although Hämäläinen et al. report good growth, no saturation experiment was present to validate these claims. In contrast to the work of Wiedmann et al., where growth was already possible starting from 150°C, growth was here only observed starting from 275°C. Increasing the substrate temperature up to 450°C also showed an increased growth rate (from 0.04 nm/cycle to 0.14 nm/cycle) and decreased chlorine content, suggesting more complete

This is the author's peer reviewed, accepted manuscript. However, the online version of record will be different from this version once it has been copyedited and typeset.

PLEASE CITE THIS ARTICLE AS DOI: 10.1063/1.50069647

reactions. This is different from the previous work, where increasing substrate temperatures showed possible decomposition. The origin of this discrepancy is not clear, although the difference in substrate (silica powder vs. planar silicon substrates) and amount of deposition cycles (20 vs. 1000) might play a role. The stoichiometry of the final films was measured to be $\text{Ti}_{0.8}\text{PO}_{3.9}$ and $\text{Ti}_{1.2}\text{P}_2\text{O}_7$ (close to stoichiometric TiP_2O_7) at 300°C and 400°C.

Titanium phosphate could also be deposited using triethylphosphate (TEP) instead of TMP. Miltzer et al.¹³ found that when TEP is pulsed directly after TiCl_4 , self-limiting growth (see figure 7(b) to illustrate self-limiting behaviour during ALD with TEP as the phosphorus precursor) at a rate of 0.22 nm/cycle could be achieved at a substrate temperature of 200°C. This novel precursor thus shows to have the highest growth rate so far, which is thought to be due to a higher reactivity than other precursors such as TMP (either through formation/decomposition into a highly reactive species in the gas phase, or just a more reactive nature of the TEP molecule itself). However, the P/Ti ratio (approximately 0.3) is lower than for other typically reported titanium phosphates deposited through ALD (0.9 to 1.7). This means that, although a higher reactivity is observed, TEP also seems to promote the formation of Ti-O bonds.

Recent developments in metal phosphate ALD using a metalorganic metal precursor. *Aluminium phosphate.* As the chlorine based metal precursors not only lead to chlorine contamination in the films, but as HCl formation could also limit the lifetime of ALD reactors and pumps, alternative options were explored. Liu et al.³¹ showed that it is possible to combine Al_2O_3 (from trimethyl aluminium, i.e. TMA, and water) with phosphorus oxide (from TMP and ozone). Using an ALD sequence of $1x(\text{TMA}-\text{H}_2\text{O}) - 20x(\text{TMP}-\text{O}_3)$ at a substrate temperature of 150°C allowed for the deposition of aluminium phosphate with a stoichiometry of $\text{Al}_{1.3}\text{PO}_{5.0}$. This composition could easily be altered by changing the number of metal oxide to phosphorus oxide cycles, but a high amount of PO_x cycles seems

This is the author's peer reviewed, accepted manuscript. However, the online version of record will be different from this version once it has been copyedited and typeset.

PLEASE CITE THIS ARTICLE AS DOI: 10.1063/1.50069647

needed to achieve a reasonable P/Al ratio. This is thought to be because of the low reactivity of TMP, even if the surface is terminated by hydroxyl groups.

The same aluminium precursor was later used in the work of Knohl et al.,³⁵ who used triethylphosphate (TEP) as their phosphorus source. It was possible to deposit an aluminium orthophosphate at 250°C, with a growth rate of 0.082 nm/cycle, but not much was investigated on the specific role of TEP as phosphorus source. It should be noted that, although the phosphorus to aluminium content is relatively low, direct reactions between the metalorganic precursor (TMA) and TMP are possible. The low P/Al ratio that is measured (0.2 – 0.3, varying from substrate to substrate) could thus be due to incomplete reactions (and using a co-reactant could enable higher ratios), or a different reaction mechanism that promotes formation of Al-O bonds (similar to the Ti-O bonds in the work of Militzer et al.).

Although TEP could be an interesting precursor to study in more detail in the future, the main focus of the deposition of phosphates is still mainly on TMP. To address the low reactivity of TMP with metalorganic precursors such as TMA (a lot of PO_x sub-cycles are needed to get a P/Al ratio close to the stoichiometric value reported in the work of Liu et al.), Hornsveld et al.³⁶ introduced an oxygen plasma, rather than water and/or ozone (i.e. TMP – O₂* - TMA – O₂*). At a substrate temperature of 150°C saturated growth was found (see figure 7(c,d,e,f) to illustrate self-limiting behaviour during ALD with TMP as the phosphorus precursor) with a growth rate of 0.18 nm/cycle. Growth was observed within a temperature window of 25°C–300°C (with a general decrease in rate with increasing temperature), but saturation was not proven over the whole window. A 1:1 sub-cycle ratio already allowed for a 0.5 P/Al atomic ratio (which is already an improvement from the work of Liu et al.), but this could easily be increased by changing the amount of PO_x sub-cycles. Omitting the oxygen plasma step after TMP still allows for thin film growth, but with a much higher P/Al ratio (0.8 vs. 0.5). TMA is thus able to react with TMP, but the oxygen plasma enables a higher reactivity (hence a higher amount of aluminium in the film).

Growth was also observed when omitting the oxygen plasma after the TMA precursor step. Although the resulting film has a very low P/Al ratio (0.13), this indicates that reactions between TMP and TMA could be possible. Unfortunately, the process without both plasma steps (i.e. TMP - TMA) was not studied. Nevertheless, it can be concluded that an oxygen plasma is not only an excellent way to remove the ligands at the surface, it also enhances the reactivity of the surface with respect to both precursors.

Iron phosphate. Apart from aluminium phosphate, Liu et al. also investigated the deposition of lithium iron phosphate,⁵⁶ and basic iron phosphate.⁷⁸ Both processes utilize a supercycle approach, in which iron oxide ($\text{FeCp}_2 - \text{O}_3$) is combined with phosphorus oxide (TMP - H_2O) and/or lithium oxide ($\text{LiO}^t\text{Bu} - \text{H}_2\text{O}$). Saturated growth was found for LiFePO_4 at a substrate temperature of 300°C with a growth per cycle of 0.94 nm/supercycle (with a supercycle consisting of 5 layers of 'iron phosphate' and one cycle of lithium oxide). Omitting the lithium oxide sub-step (i.e. $\text{FeCp}_2 - \text{O}_3 - \text{TMP} - \text{H}_2\text{O}$) still allowed for growth with a rate of 0.075 nm/cycle. Growth of non-lithiated iron phosphate was evaluated in a broader temperature range, showing an overall increase of the growth rate from 0.02 nm/cycle to 0.06 nm/cycle when the substrate temperature increases from 200°C to 350°C . The P/Fe ratio also showed a decrease, which was thought to be due to thermal activation of the iron oxide process, while the phosphorus oxide process step was less affected.

Chernyaeva et al.⁵⁸ also attempted the deposition of LiFePO_4 , using a pulsing sequence of $\text{LiO}^t\text{Bu} - \text{H}_2\text{O} - \text{FeCl}_2 - \text{H}_2\text{O} - \text{TMP} - \text{H}_2\text{O}$. Deposition proved possible at 300°C , but no saturation and/or growth rate are reported. However, the reaction time needed for each precursor to react with an -OH terminated surface was measured using Scanning Probing Microscopy (SPM). From this, it was seen that both reactions of LiO^tBu and FeCl_2 are taking place reasonably fast, but reactions of TMP with an -OH terminated surface is going extremely slow. This was also seen by the initially low P/Fe ratio (0.19), which could be increased with increasing pulse times (0.31). This shows that, as was expected from other

This is the author's peer reviewed, accepted manuscript. However, the online version of record will be different from this version once it has been copyedited and typeset.

PLEASE CITE THIS ARTICLE AS DOI: 10.1063/1.50069647

work, reactions of TMP (with for example -OH terminated surfaces) are typically much slower than the other surface reactions used in the deposition process. One does need to be careful in forming a final conclusion based on solely these results, as a lot of information on the process parameters (such as precursor temperature, and the use of a potential carrier gas) are missing.

Gandrud et al.⁵⁹ and Brennhagen et al.⁶⁰ also successfully deposited (non-lithiated) iron phosphate, but this was done by using $\text{Fe}(\text{thd})_3$ as iron precursor rather than FeCp_2 or FeCl_2 . The deposition process $\text{Fe}(\text{thd})_3 - \text{O}_3 - \text{TMP} - (\text{H}_2\text{O} + \text{O}_3)$ in the work of Gandrud et al. showed an increasing amount of iron content with increasing substrate temperature (similar to the work of Liu et al.⁷⁸), while the growth per cycle is more or less stable at 0.05 nm/cycle (for a 1:1 cycle ratio) in the 246°C–360°C temperature window. Brennhagen et al. only focussed on a substrate temperature of 250°C at which they varied the cycle ratio allowing for P/Fe ratios close to stoichiometric FePO_4 and $\text{Fe}_4(\text{P}_2\text{O}_7)_3$.

Lanthanum phosphate. The inclusion of a mixed $\text{H}_2\text{O} + \text{O}_3$ co-reactant pulse was based on the work of Sønsteby et al.,⁶² who used $\text{La}(\text{thd})_3$ and TMP to investigate the deposition of lanthanum phosphate. Growth of the deposition process $\text{La}(\text{thd})_3 - \text{O}_3 - \text{TMP} - (\text{H}_2\text{O} + \text{O}_3)$ was possible, with a stable growth rate of 0.078 nm/cycle in the 250°C–300°C temperature window. Self-limiting behaviour of each precursor pulse was found at a substrate temperature of 275°C. Without O_3 after the $\text{La}(\text{thd})_3$ pulse, film growth is not possible, indicating that TMP is unable to react with the thd-ligand, and that it prefers reactions with the surface after a highly reactive co-reactant step. However, the combined ($\text{H}_2\text{O} + \text{O}_3$) pulse was able to achieve self-limiting growth with controllable phosphorus content. Unfortunately the nature of the reactions, and the exact reason as to why both co-reactants have to be used, was not investigated in detail. Doping lanthanum phosphate with calcium was also proven to be possible in this work, by replacing $\text{La}(\text{thd})_3$ by $\text{Ca}(\text{thd})_2$ every 19th cycle.

Tin phosphate. The need for a highly reactive co-reactant after the TMP pulse was also discussed by Park et al,⁴¹ who reported deposition of tin phosphate using TDMASn and TMP. In this work, TMP was pulsed directly after TDMASn, but ozone was needed after the TMP process step for successful deposition. If water was used instead of ozone, the growth rate was only 0.01 nm/cycle at a substrate temperature of 250°C and no phosphorus was present in the film. Using only ozone did allow for phosphorus incorporation and an increased growth rate (0.12 nm/cycle and P/Sn atomic ratio of 0.05), but pulsing both co-reactants after each other (H₂O – O₃ pulse) allowed for the highest growth rate (0.18 nm/cycle) and P/Sn atomic ratio (0.17). This was explained by possible water adsorption in the initial step, which increased the probability for the TMP molecules to be combusted by O₃. This is again pointing towards two different mechanisms in the combustion process of the adsorbed TMP molecules, in which ozone is needed for growth of the phosphate, and water can help to enhance the hydroxylation.

Europium phosphate. Using Eu(thd)₃ as metal precursor, europium phosphate could be deposited by Getz et al.⁷⁹ This was done by combining sub-cycles of europium oxide (Eu(thd)₃ – O₃) with phosphorus oxide (TMP – (H₂O + O₃)). The mixed water/ozone step was based on previous work, and not further investigated. At a substrate temperature of 300°C, growth was observed with a rate of 0.1 nm/cycle. For improved luminescence properties, this was mixed with a titanium phosphate from the TiCl₄ – H₂O – TMP – (H₂O + O₃) process. The growth per cycle at a substrate temperature of 300°C was 0.08 nm/cycle, which is lower than what was found in the work of Wiedmann et al. (0.12 nm/cycle at 250°C). This could be due to a difference in substrate nature, or due to the inclusion of ozone in the process. It is not thought to be due to the higher substrate temperature, as the growth per cycle in the latter work showed an increasing trend as a function of temperature rather than decreasing.

This is the author's peer reviewed, accepted manuscript. However, the online version of record will be different from this version once it has been copyedited and typeset.

PLEASE CITE THIS ARTICLE AS DOI: 10.1063/1.50069647

Zinc phosphate. The possibility for the deposition of zinc phosphate was first introduced by Yuan et al.,⁶³ who investigated phosphorus doping of zinc oxide. In this work, diethylzinc (DEZ) was introduced in the ALD chamber together with TMP. The deposition process DEZ/TMP – O₃ allowed for the growth of phosphorus doped zinc oxide (growth rate of 0.17 nm/cycle) at a substrate temperature of 250°C. Altering the TMP/(DEZ + TMP) pressure ratio then allowed for an increase in phosphorus content up to 3 at.%. This was not included in table 1, as no clear P/Zn ratios were mentioned and the mixing of both precursors does not allow to determine a ‘pulsing’ ratio. Saturation of this process was not tested, which questions its self-saturating behaviour. Next to this, as the amount of incorporated phosphorus is very low, the resulting layer is clearly a zinc oxide doped with a low amount of phosphorus rather than a zinc phosphate.

In the work of Tynell et al.,⁶⁴ the DEZ and TMP pulses were split up, to end up with a DEZ – H₂O – TMP – H₂O deposition process at a substrate temperature of 160°C. By varying the amount of DEZ – H₂O to TMP – H₂O pulses, the dopant level was increased from 0 at.% to 5 at.%. With this increase, a decrease in growth rate from 0.19 nm/cycle to 0.16 nm/cycle was found. Apart from a slower growth rate of the phosphorus oxide in comparison to zinc oxide, it was thought that P-doping somewhat hindered the further zinc oxide growth. This is possible, as it was seen from the work of Wiedmann et al. that water does not fully react away all methyl groups which could then hinder further growth (as, unlike TiCl₄, DEZ does not react with methyl groups). However, the amount of phosphorus is still too low to be able to call it a phosphate.

Cobalt phosphate. A deposition process for cobalt phosphate was developed by Di Palma et al.,⁶⁶ based on the cobalt oxide deposition CoCp₂ – O₂*, where the star again denotes a plasma. In a 1:1 combination with TMP – O₂*, self-limiting growth of cobalt phosphate was found at a substrate temperature of 300°C with a growth rate of 0.11 nm/cycle. A stoichiometry of Co_{3.2}P₂O₉ was found, which is close to the theoretical Co₃P₂O₈. A more

This is the author's peer reviewed, accepted manuscript. However, the online version of record will be different from this version once it has been copyedited and typeset.

PLEASE CITE THIS ARTICLE AS DOI: 10.1063/1.50069647

cobalt rich phosphate could be obtained, by increasing the amount of $\text{CoCp}_2 - \text{O}_2^*$ to $\text{TMP} - \text{O}_2^*$ sub-cycles. Although not discussed in this work, cobalt oxide could also be deposited by using ozone instead of an oxygen plasma.⁸⁰ If a plasma is preferably avoided, the knowledge from other depositions could thus be used in future work to investigate for example a $\text{CoCp}_2 - \text{O}_3 - \text{TMP} - (\text{H}_2\text{O}$ and/or $\text{O}_3)$ process.

Sodium phosphorus oxynitride. Deposition of nitrogen doped sodium phosphate was investigated by Nuwayhid et al.,⁷⁰ who combined DEPA vapour with NaO^tBu . Growth of a sodium phosphorus oxynitride was found (similar to the lithium phosphorus oxynitrides mentioned earlier) at a deposition temperature ranging from 300°C to 400°C. With increasing temperature, the growth rate increased from 0.01 nm/cycle to 0.1 nm/cycle, although the high temperature lead to non-ideal ALD growth (poor saturation of the NaOtBu precursor). The need for such high temperatures with respect to the similar LiPON process of Pearse et al. is thought to be the more complex nature of reactions involving NaO^tBu .

Magnesium phosphate. Su et al.¹⁹ deposited magnesium phosphate using $\text{Mg}(\text{EtCp})_2$ and TDMAP ($\text{Mg}(\text{EtCp})_2 - \text{H}_2\text{O} - \text{TDMAP} - \text{O}_2^*$). In the 125°C–300°C temperature window, the growth per cycle decreased from 0.14 nm/cycle to 0.12 nm/cycle and the P/Mg ratio decreased from 0.82 to 0.67. At 250°C saturated growth was observed, which is illustrated in figure 7(g,h), showing the self-limiting behaviour during ALD with TDMAP as the phosphorus precursor. From the FTIR spectra at different precursor exposures (figure 6(a,b)), the presence of a Mg - O - P peak confirmed the formation of a Mg phosphate at high enough exposure times for both precursors. TDMAP was chosen as the phosphate precursor to possibly enable the formation of a magnesium phosphorus oxynitride (nitrogen doped magnesium phosphate) through its dimethylamino ligands. However, the oxygen plasma showed to burn away all the nitrogen, leading to the deposition of the undoped metal phosphate. If deposition of a phosphorus oxynitride is desired, the oxygen plasma could for example be

This is the author's peer reviewed, accepted manuscript. However, the online version of record will be different from this version once it has been copyedited and typeset.

PLEASE CITE THIS ARTICLE AS DOI: 10.1063/1.50069647

replaced by a nitrogen plasma, as will be discussed later.

Plasma polymerisation for rapid metal phosphate ALD. Dobbelaere et al.²¹ circumvented the stability of TMP (which makes it such a popular and easy-to-handle precursor, but also implies low reactivity) by turning it into a plasma, effectively producing a thin phosphoric acid layer on the sample surface through self-limited plasma polymerisation. At a low substrate temperature (below 300°C), the plasma-activated TMP leads to non-saturated growth of a PO_x layer. At temperatures above 300°C, this so called 'plasma polymerisation' became self-limiting, meaning that TMP plasma (TMP*) was not able to deposit a film by itself. This is illustrated in figure 8(a), where the decomposition rate of TMP* (defined as the amount of growth per second due to TMP* exposure) shows to decrease with increasing substrate temperature, finally inhibiting continuous growth beyond one monolayer at 300°C. As the resulting monolayer is partially terminated by hydroxyl groups, a combination with a metalorganic precursor such as TMA is able to re-initiate growth, allowing for the deposition of aluminium phosphate through a TMP* - TMA process. Inclusion of an oxygen plasma directly after the TMP* process step further hydroxylized the phosphate esters, burning away the remaining methyl ligands and enhancing the reactivity towards TMA even more. This final TMP* - O_2^* - TMA process then leads to the saturated deposition of an aluminium pyrophosphate (P/Al atomic ratio of 1.8), with a growth rate of 0.37 nm/cycle at a deposition temperature of 320°C. Using the fact that aluminum oxide can be deposited using a O_2^* - TMA process, more aluminium rich layers could potentially also be deposited by using multiple aluminium oxide sub-cycles per TMP* sub-cycle (similar to the metal oxide - phosphorus oxide intermixing mentioned earlier). The TMP-plasma based approach process that was proposed in this work is thus able to rapidly (highest growth rate of all reports) deposit a phosphorus rich aluminium phosphate with a decreased process complexity, without the need for lengthy super cycles, and without (hypothetically) sacrificing tunability of the composition.

This is the author's peer reviewed, accepted manuscript. However, the online version of record will be different from this version once it has been copyedited and typeset.

PLEASE CITE THIS ARTICLE AS DOI: 10.1063/1.50069647

More importantly, this plasma based process could easily be extended towards other metal phosphates by changing the metal precursor. When TMA is for example replaced by tert-butyl ferrocene (TBF),⁶¹ iron phosphate (P/Fe atomic ratio of 1.5) could be deposited with a very high growth rate of 1.1 nm/cycle at a temperature of 300°C. The use of diethylzinc (DEZ)⁶⁵ allowed for the formation of zinc phosphate (P/Zn atomic ratio of 2.2) with a growth rate of 0.92 nm/cycle at the same substrate temperature. Titanium phosphate⁵⁴ could also be deposited at 300°C at a rate of 0.66 nm/cycle (P/Ti atomic ratio of 1.7) by using TTIP as the metal source. The use of TEMAV as the metal source allowed for the deposition of vanadium phosphate,⁶⁹ at a growth rate of 0.78 nm/cycle (P/V atomic ratio of 0.88). The latest material that has been published using this technique is a cobalt phosphate,⁶⁸ which was deposited at a growth rate of 0.8 nm/cycle, again at a substrate temperature of 300°C (P/Co atomic ratio of 2.3). Using this technique, a large number of metal phosphates could thus be deposited with a very high growth rate and P/M ratio with respect to other processes, showing the high reactivity of the TMP plasma species. To further illustrate the self-saturating behaviour of these plasma enhanced processes, the growth per cycle measured during the growth of titanium phosphate⁵⁴ is presented in figure 8(b).

Plasma polymerisation for nitrogen doping of metal phosphates. Alternatively, Henderick et al.³⁷ investigated plasma polymerisation based approaches for the deposition of nitrogen doped metal phosphates. In a first approach, the process proposed by Dobbelaere et al. was altered by replacing the oxygen plasma by a nitrogen plasma (i.e. TMP* - N₂* - TMA). This allowed for the incorporation of approximately 8 at.% of nitrogen, with a growth per cycle of 0.8 nm/cycle.

Alternatively, inspired by the dual-source nature of DEPA (which has both nitrogen and P-O bonds) and its similarities with respect to TMP, the plasma polymerisation of DEPA and its potential use as a PE-ALD phosphorus precursor were studied. A similar plasma polymerisation effect (PE-CVD at low temperature, self-limiting PE-ALD at high tempera-

This is the author's peer reviewed, accepted manuscript. However, the online version of record will be different from this version once it has been copyedited and typeset.

PLEASE CITE THIS ARTICLE AS DOI: 10.1063/5.0069647

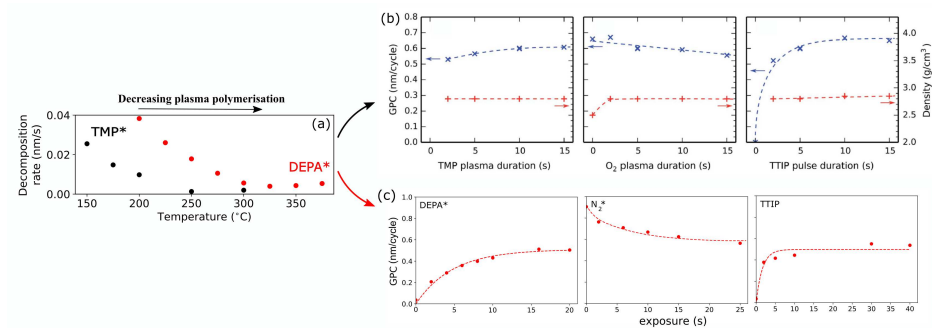


Figure 8: (a) The decomposition rate (defined as the amount of growth per second of exposure of the precursor in question) of TMP* and DEPA* at different substrate temperatures. Adapted with permission from [55]. Copyright 2021 Elsevier. (b) Saturation of all three precursors in the TMP* - O₂* - TTIP process at 300°C for the deposition of titanium phosphate.⁵⁴ Adapted with permission from [54]. Copyright 2016 Royal Society of Chemistry. (c) Saturation in the DEPA* - N₂* - TTIP process at 300°C for the deposition of nitrogen doped titanium phosphate.⁵⁵ Adapted with permission from [55]. Copyright, 2021 Elsevier.

ture, see figure 8(a)) as TMP was found, allowing for a nitrogen doped aluminium phosphate to be deposited by the DEPA* - N₂* - TMA process.³⁷ The very high growth rate of 1.4 nm/cycle at a substrate temperature of 325°C was thought to be due to the incorporation of lengthy triply coordinated nitrogen bonds (nitrogen bound to three phosphorus atoms instead of two).

Later, this process was also used for the deposition of (nitrogen doped) titanium phosphate, by replacing the TMA precursor by TTIP at a substrate temperature of 300°C.⁵⁵ Nitrogen doped titanium phosphate (with approximately 9 at.% of nitrogen) could be deposited with a growth rate of 0.6 nm/cycle when DEPA* is used as the phosphorus source. The self-saturating behaviour was proven by measuring the growth per cycle as a function of precursor exposure, as presented in figure 8(c).

Deposition of PO_x (phosphorus oxide) layers. It does need to be noted that, although they are not typical (metal) phosphates such as the materials discussed previously, the growth of PO_x layers also gained interest. In the work of Black et al.,⁷¹ an InP substrate

This is the author's peer reviewed, accepted manuscript. However, the online version of record will be different from this version once it has been copyedited and typeset.

PLEASE CITE THIS ARTICLE AS DOI: 10.1063/1.50069647

was alternately exposed to TMP and O_2^* pulses, forming a PO_x -interlayer at a growth rate of 0.11 nm/cycle. As the phosphorus oxide layer is unstable in air, an Al_2O_3 capping layer had to be applied, making this in essence a very extreme case of the process reported in the work of Hornsveld et al. Instead of intermixing a metal oxide with a phosphorus oxide for the deposition of a metal phosphate, this work aims towards clearly separated regions. The substrate temperature of 25°C and the lack of saturation experiments, however, do question the self-saturating nature of the reported process.

A similar approach was used in the work of Kalkofen et al.,⁷³ who combined hexamethyl-triaminophosphine (HMPT, actually the same molecule as the earlier described TDMAP) with O_2^* for the deposition of phosphorus oxide on silicon. As this was again very unstable in air, intermixing the PO_x -layer (now deposited using TEP instead of HMPT) with silicon oxide ($Si(N(Me_2)_3 - O_2^*)$), and thus the deposition of silicon phosphate, was investigated. However, The information on the reported processes is quite scarce, and more research is needed to study the deposition of silicon phosphate.

Phosphorus oxide was also deposited by Knemeyer et al.,⁷² combining trimethoxy phosphine (TMPT) as the phosphorus source with oxygen. At a substrate temperature of 150°C, growth is only observed in the first few cycles. Increasing the substrate temperature to 450°C allowed for linear growth during the first ten cycles, but growth beyond this limit was not discussed. The growth of this phosphorus oxide layer is thought to be depending on the substrate (vanadium oxide), as the proposed reaction mechanism utilises the oxidation of phosphorus together with a reduction of the vanadium atoms.

From these reports, it can be seen that there has been a lot of research already on the topic of ALD of phosphates. Typical problems involve a relatively low growth rate and/or a low amount of phosphorus (lower than the expected stoichiometric value) in the final layer. Multiple techniques and precursors have been proposed to achieve the desired concentration/reactivity, of which each has their own (dis)advantage. The next section aims at a concise overview of the proposed reaction mechanisms involved in the abovementioned

reports.

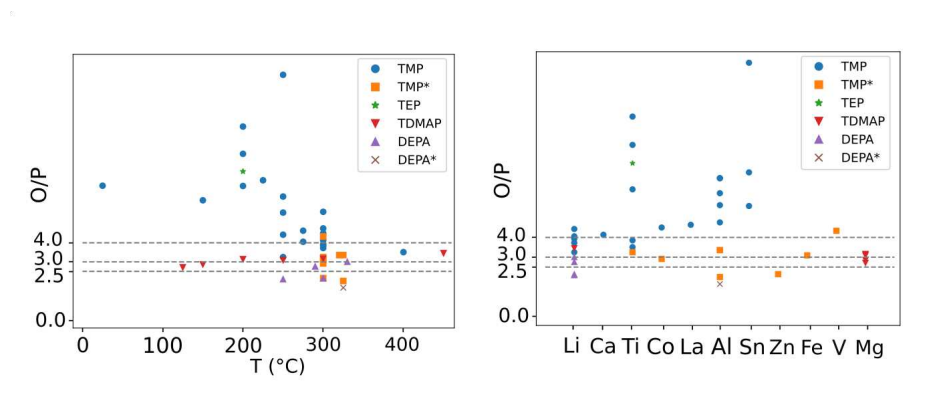


Figure 9: Data from Table 1, from selected papers where full composition is reported. If supercycles were used, we selected the data with 1:1 ratio between phosphate/metal cycle. The same data is plotted in the two graphs. Both the substrate temperature and the choice of precursor strongly affect the P/O ratio in the film (see text). Data from ^{13,19,21,28-31,33,36,37,39,41,42,50,52-54,61,62,65,66,68,69}

Variation of phosphate connectedness based on reaction conditions

From the materials reported in Table 1, we selected those for which complete XPS,^{13,19,21,28,30,31,37,41,50,53,54,61,62,65,69} ERD^{21,29,36,37,39,42,54,61,66,68,69} or RBS^{33,36,52,66} quantification data were available. As discussed before, one can argue that the lower the O/P ratio, the more connected the phosphate is (the more P-O-P bindings we have) (Fig. 1). It may vary from 2.5 (fully interconnected phosphate) to 4 (all phosphate units are connected at all sides to another metal). However, there is no reason to stop at 4: if the oxygen content raises further, it means that the metal oxide starts forming structures on its own. All these phosphate flavors can be observed in Fig. 9. In the following, we will discuss the effects of temperature, precursor and pulsing sequence on the connectedness of the resulting phosphates.

Effect of temperature on connectedness

It can be readily observed from Fig. 9, that often an elevated temperature is necessary to deposit actual phosphates. Several processes only work at elevated temperatures, while those that report growth at lower temperatures often rather describe deposition of phosphorus-doped metal oxides.

Effect of the phosphate precursor on connectedness

More striking than the temperature effect, which is to some extent expected when using quaternary processes at different temperatures, is the effect the precursor has on the connectedness between the phosphate units (fig. 9 right). We can clearly see the effect of the fourfold O coordination in the TMP (and TEP) molecule: the PO_4 unit is already present, and from the available literature there are no signs of polymerisation reactions that can take place. Although it could be possible through for example the formation of dimethyl ether, the polymerisation appears to be rather unlikely at the conditions used in the ALD processes presented here. There might be various reaction pathways at e.g. more elevated temperatures, but decomposition of the precursors might become an issue there. The difficulty of polymerising two TMP molecules is particularly clear from additional experiments that were conducted for this review article. It was found that, using a set-up similar to the one used by Dobbelaere et al.,²¹ no growth is observed after 225 cycles of TMP - O_2^* at a substrate temperature of 300°C, proving that growth beyond the TMP unit is rather difficult and that the linking of phosphorus atoms has to happen via metal atoms at the given temperature. Excess oxygen may arise from metal atoms joining among each other. This is the reason that the subcycle approach with thermal TMP processes works only when the P/M ratio is to be decreased.

The situation is different when TMP (or DEPA, although this typically results in a phosphorus oxynitride rather than a phosphate) is polymerized in the plasma. These processes are not only remarkable because of their exceptionally high growth per cycle. As implied in the

name plasma polymerization and described in the previous section, the phosphate units get joined in the plasma, opening up a new part of the parameter space for TMP: with plasma polymerization, PO_4 units can get interconnected. It seems that there is some variation in connectedness, and it would be interesting to see how plasma parameters such as power, flow and pressure of both plasma pulses affect the network characteristics of the deposited layer.

A similar network forming without plasma polymerization is described with the TDMAP precursor. Note that it naturally seems to evolve towards 3 oxygen atoms per phosphorus atom. However, in the course of the deposition, the oxidation state of the P atom changes from III to V due to an oxygen plasma pulse, and an O/P ratio of 3 is only due to the cross-linking of PO_4 structures (on average 2 units are connected). A similar change in P valence from III to V in the trimethylphosphite precursor ($\text{P}(\text{OCH}_3)_3$) was described by Kvamme⁸¹ in his master thesis and in ref.⁷² The trimethylphosphite approach may yield similar results to the trimethylphosphate. Here, the 3 bridging oxygens are already specified, and an additional oxygen might be further provided by an oxygen-containing pulse. The oxygen-containing precursor would in that case lead to phosphorus oxidising towards the most stable P(V). However, it does need to be noted that more research is needed to verify this.

Effect of pulsing sequence and subcycles on connectedness

While in glass science it is quite convenient to mix materials in a stoichiometric manner, in ALD research this is usually not that easy. In the ideal case, each atomic constituent of the film arrives in its own organic package. While it is possible to tune the P/M ratio by modifying the number of subcycles, this most often is done only in one direction, decreasing the number of phosphorus groups in favor of the metal oxide, which quickly becomes the backbone. Furthermore, as discussed before, in the case of TMP, a precursor molecule may come in preformed units. If no additional metal is to be supplied, the reactant should thus not only be able to remove organic ligands, but as well to connect these preformed units or make a joint by removing oxygen atom. This is an interesting observation as well with regard

to precursors for other materials. For example, if one aims to deposit TiO₂ with titanium isopropoxide, it should be noted that in this particular precursor a TiO₄ unit is present, and that two oxygen atoms need to be removed in order to deposit stoichiometric TiO₂. We also note that when applied to deposition of ternary or quaternary oxides, selection of a precursor with a specific unit can be of great help to control the joints of the network.

ALD mechanism

With the different deposition processes summarized in the previous sections, an attempt can now be made to get a good understanding of the reaction mechanism that allows for the deposition of phosphates. In the following section, different types of reaction schemes that allow for metal phosphate deposition will be discussed by using aluminum phosphate as a general case study. The deposition of other metal phosphates will only be discussed if they can provide additional insights into the deposition process under discussion. It does need to be noted that some of the reaction mechanisms are just proposed (based on the available data), and do need experimental confirmation.

ALD using phosphoric acid. If phosphoric acid could be vaporised, it would serve as an ideal candidate for metal phosphate deposition. The hydroxyl termination could easily be combined with metalorganic precursors such as TMA, resulting in a reaction scheme similar to the well known TMA - H₂O process. The hypothetical reactions that could take place during the deposition of aluminum phosphate using phosphoric acid are shown in figure 10(a). However, as explained earlier, phosphoric acid cannot be efficiently vaporised meaning that other deposition mechanisms have to be investigated.

ALD using PCl₃ and P₂O₅. The first precursor that allowed for successful deposition of a metal phosphate, PCl₃, had to be combined with water to allow for the formation of a P₂O₅ monolayer. Combining this phosphorus oxide layer with a metal oxide allowed for the

This is the author's peer reviewed, accepted manuscript. However, the online version of record will be different from this version once it has been copyedited and typeset.

PLEASE CITE THIS ARTICLE AS DOI: 10.1063/1.50069647

formation of the metal phosphate. This particular deposition process was reported for the deposition of titanium phosphate,²⁷ but the reaction mechanism could be extended to its use for the aluminum phosphate case. Although the nature of the reaction between PCl_3 and water was never reported, a reaction similar to for example TiCl_4 and water can be expected. This means that water could react with the -Cl terminated groups by the formation of HCl, leaving behind -OH terminated groups for a metal precursor to react with. If one would hypothetically use AlCl_3 as the aluminum source (in line with the reported deposition of titanium phosphate, using TiCl_4), a reaction mechanism as presented in figure 10(b) could allow for the deposition of aluminum phosphate. One could potentially also use metalorganic precursors such as TMA to react with the hydroxyl groups, but this is not presented here. To step away from the toxicity of PCl_3 , P_2O_5 was introduced as a new source for the phosphorus in combination with AlCl_3 as the aluminum source. Although not much is known about the mechanism of the P_2O_5 reactions, it was found that an -OH terminated surface was needed for P_2O_5 to react to. If such a surface is present, a relatively high reactivity was found based on the amount of phosphorus (P/Al atomic ratio). A possible explanation for the observed reactions could be the formation of a thin phosphoric acid layer through reactions with the -OH terminated groups and/or the subsequent water pulse. As phosphoric acid is reactive towards the typical metal precursor (through its -OH termination), further reactions can proceed. However, as P_2O_5 has to be heated to very high temperatures, the precursor was not used anymore and the reaction mechanism was not studied any further.

Reaction mechanisms using trimethyl phosphate as the phosphorus source. TMP can be evaporated fairly easy. Its stability, however, complicates the processes and reaction mechanisms that are needed for successful deposition of the desired phosphate. To avoid the low reactivity of its $-\text{CH}_3$ ligands towards different metalorganic precursors (such as TMA), the majority of the reports rely on reactions between TMP with chlorine based groups and/or hydroxyl based groups. There is a clear exception for lithium phosphate (which will be dis-

This is the author's peer reviewed, accepted manuscript. However, the online version of record will be different from this version once it has been copyedited and typeset.

PLEASE CITE THIS ARTICLE AS DOI: 10.1063/1.50069647

cussed separately), as well as a few other non-lithium phosphate depositions where chlorine or hydroxyl groups were not needed.

Chlorine based metal precursors. The first group of reactions is enabled by using a chlorine based metal precursor such as AlCl_3 or TiCl_4 . Growth has been observed in multiple occasions without the need of an extra co-reactant pulse after the metal precursor, showing successful reactions between chlorine and $-\text{CH}_3$ ligands. In the work of Wiedmann et al., this was explained by the formation of CH_3Cl during both (phosphorus and metal) precursor pulses, leaving behind either a $-\text{CH}_3$ terminated surface (after the TMP pulse) or a $-\text{Cl}$ terminated surface (after the TiCl_4 pulse). If one would extend this knowledge to the discussion of aluminum phosphate, a reaction mechanism as presented in figure 10(c) could be expected for the deposition reported by Hamalainen et al.²⁹ However, it is important to notice that Wiedmann et al. did not observe saturation in the simple TiCl_4 – TMP process. They expected this to be due to ligand exchange at the surface, forming thermally unstable TiCl_xMe_y surface species which will lead to non-saturated growth. The addition of water as a co-reactant (either after the TiCl_4 pulse and/or after the TMP pulse) showed to result in more saturated growth, which was explained by looking at the reaction mechanism in more detail using mass spectrometry. The water pulse after TiCl_4 resulted in a surface terminated by $-\text{OH}$ groups, through the formation of HCl . The subsequent TMP pulse then showed to primarily react with the un-reacted $-\text{Cl}$ surface species (rather than with the hydroxyl ligands), after which a small amount of CH_3OH was detected during the last water pulse (showing slow combustion of $-\text{CH}_3$ into $-\text{OH}$ surface species). In the next ALD cycle, the TiCl_4 then reacts with both the $-\text{OH}$ and $-\text{CH}_3$ ligands to continue further growth. The more stable bonds in the surface that was partially hydroxylized (due to the inclusion of water in the process) then resulted in saturated growth as they are not as thermally unstable as the previously mentioned TiCl_xMe_y surface species. Although such a detailed study was not yet performed for the aluminum phosphate case, one could similarly expect that the reactivity of

This is the author's peer reviewed, accepted manuscript. However, the online version of record will be different from this version once it has been copyedited and typeset.

PLEASE CITE THIS ARTICLE AS DOI: 10.1063/1.50069647

TMP might be higher towards chlorine based groups rather than towards hydroxyl groups, but the latter are thought to result in a more stable surface. Unfortunately, the use of water leads to the formation of HCl, which can harm the ALD equipment, and etch the deposited material. It is thus better to look for reaction mechanisms that lead to stable growth, without the formation of side products such as HCl. This could be done by using a metalorganic precursor such as TMA, and look for the most appropriate mechanism to combine it with TMP.

Thermal co-reactants for metalorganic precursor based ALD processes. If chlorine based metal precursors are avoided, hydroxylation of the surface prior the TMP pulse has shown to positively impact the interactions between TMP and a metalorganic precursor. Even more important, most of the reports seem to imply that direct reactions of for example a methyl-ligand and/or a thd-ligand (thd = 2,2,6,6-tetramethyl-3,5-heptanedionato) with TMP are not possible. Inclusion of a water, oxygen plasma and/or ozone process step after the metal precursor is needed in a lot of cases for the complex ligands to be replaced by -OH groups,³⁶ and for the gas molecules in the subsequent TMP pulse to react with the surface. This has been particularly clear in the work of Sønsteby *et al* who found that without an ozone process step in between La(thd)₃ and TMP, growth is not possible. The fact that all reports in which a metalorganic precursor is combined with TMP prefer to make use of such a co-reactant pulse prior to the TMP pulse, further highlights the importance of surface hydroxylation. However, although reactions between TMP and a hydroxylized surface show to be possible, they do appear to be rather slow (as described in the work of Chernyaeva *et al.*⁵⁸). Most processes relying on these reactions with TMP eventually show low P/M ratio's and low growth rates. If one includes multiple PO_x sub cycles, the P/M ratio could be increased but the process becomes more lengthy and complex.

All of these processes also prefer the use of a hydroxylating co-reactant after the TMP pulse. This again highlights the importance of hydroxylating the surface, enhancing its reactivity

This is the author's peer reviewed, accepted manuscript. However, the online version of record will be different from this version once it has been copyedited and typeset.

PLEASE CITE THIS ARTICLE AS DOI: 10.1063/5.0069647

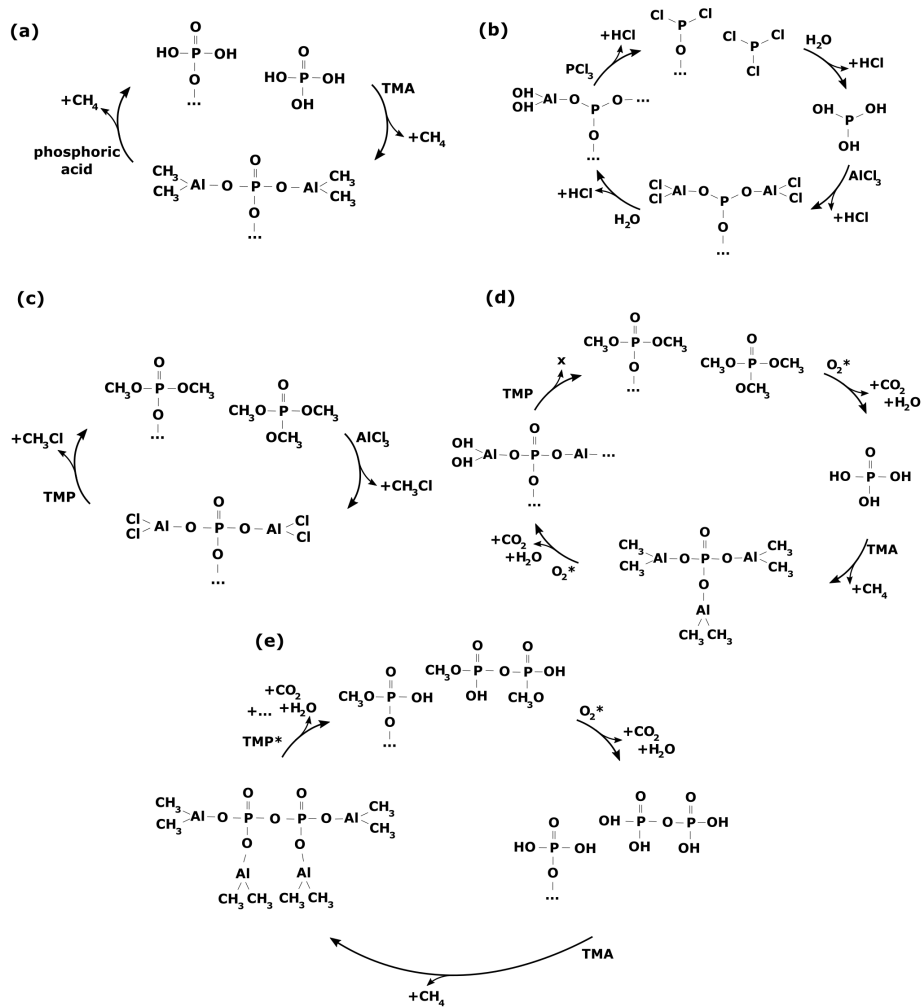


Figure 10: Illustration of several selected deposition mechanisms for aluminum phosphate using (a) phosphoric acid, (b) PCl₃, (c) TMP with a chlorine based metal precursor, (d) TMP with a metalorganic precursor and (e) plasma polymerisation of TMP. Some of these processes are merely the suggested mechanisms and need experimental confirmation.

towards reactions involving both TMP and a metalorganic precursor. However, the nature of the co-reactant and its interactions with the surface terminated by for example adsorbed

This is the author's peer reviewed, accepted manuscript. However, the online version of record will be different from this version once it has been copyedited and typeset.

PLEASE CITE THIS ARTICLE AS DOI: 10.1063/1.50069647

TMP molecules is still up for debate. It was for example found in the work of Sønsteby *et al* that the most efficient growth of lanthanum phosphate was observed when a $\text{H}_2\text{O} + \text{O}_3$ mixture was pulsed after the TMP pulse instead of only O_3 or only H_2O . It was suggested that in this combined co-reactant, two underlying but separate mechanisms are involved in terminating the phosphate groups. It is for example possible that water releases the methyl groups from the TMP, while ozone creates surface sites that are more suited for reactions with $\text{La}(\text{thd})_3$. The general importance of such a combined co-reactant pulse is not yet clear, as only water showed to be sufficiently reactive in the work of Ananda Sagari *et al.* and Putkonen *et al.*, who encountered a thd-ligand in $\text{Ca}(\text{thd})_2$. As it is not clear if pulsing only water or only ozone showed good growth in the work of Gandrud *et al.* (who used such a combined co-reactant pulse for their iron phosphate deposition), it cannot be concluded if this mechanism is needed for thd-ligands in general, or the $\text{La}(\text{thd})_3$ in particular. Next to not fully understanding the possible impact of the combined co-reactant pulse, the potential effects for other metalorganic precursors has not yet been investigated. The importance of surface hydroxylation is thus clear, but the nature of the co-reactant that is used for this cause might depend on the metal precursor of choice.

It appears that there is no need for an additional hydroxylating co-reactant when TEP is used as the phosphorus source, which is relatively similar to TMP. In the work of Knohl *et al.*,³⁵ aluminum phosphate was deposited from direct reactions between TEP and TMA. As not much was discussed on the role of TEP, and the possible (positive) impact of an additional co-reactant, we suggest that a more detailed investigation is needed before any conclusions on the reaction mechanisms can be made.

Lithium phosphate based ALD processes. The deposition of lithium phosphate processes using TMP as the phosphorus source shows to be a clear exception on the need for co-reactants in between TMP and the metal precursor. In these processes, most reports (regarding lithium phosphate without nitrogen doping) use direct reactions between a lithium precursor such

This is the author's peer reviewed, accepted manuscript. However, the online version of record will be different from this version once it has been copyedited and typeset.

PLEASE CITE THIS ARTICLE AS DOI: 10.1063/5.0069647

as LiHMDS or LiO^tBu and TMP. The direct reactions between LiHMDS and TMP were studied in more detail by Werbrouck et al.,⁴⁵ resulting in an interesting reaction mechanism proposed for this process (figure 11). Assuming the surface before the LiHMDS-TMP cycle is terminated by O-Li groups from the lithium phosphate, no reaction products were observed in a mass spectrometer during the LiHMDS pulse. It was expected that a dipole-dipole interaction between the O-Li at the surface and the N-Li in the precursor allowed for physisorption of the entire molecule. The complex ligands of the molecule then screened the surface dipoles inhibiting further growth (i.e. the pulse is self-limiting). In the subsequent TMP pulse, the lithium from the physisorbed molecule as well as the phosphate anion are built into the film while the HMDS and methyl groups are removed through the formation of CH_3HMDS . It was also found that TMP molecules not only interacted with the surface through a ligand exchange with the physisorbed LiHMDS molecules, but that the TMP molecule could also simply physisorb on the surface without the formation of byproducts (which was expected to be due to a similar dipole-dipole interaction). Although the entire

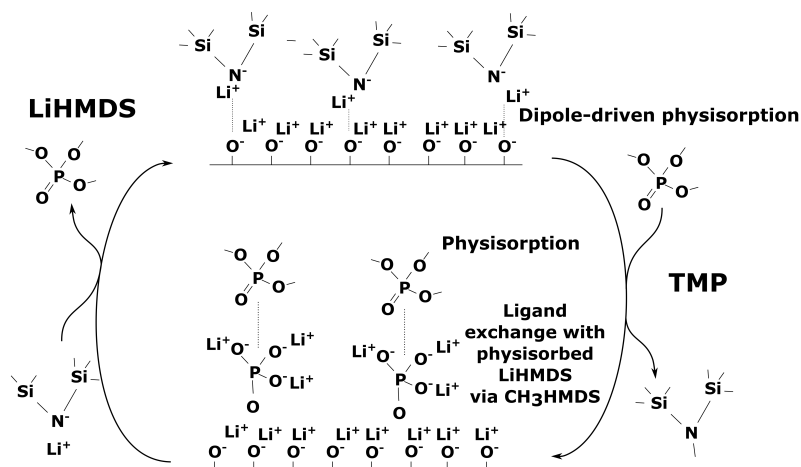


Figure 11: Illustration of the reaction mechanism in a LiHMDS-TMP process. Adapted with permission from [45]. Copyright 2020 American Chemical Society.

This is the author's peer reviewed, accepted manuscript. However, the online version of record will be different from this version once it has been copyedited and typeset.

PLEASE CITE THIS ARTICLE AS DOI: 10.1063/1.50069647

TMP molecule was seen to be removed in the following LiHMDS pulse (i.e. physisorbed TMP did not interact with LiHMDS at the surface) and did thus not participate any further in this particular process, the introduction of such a potential reaction pathway could help to gain further insight in TMP-based ALD processes. Nevertheless, with this work it was clearly shown that an ALD lithium phosphate process is possible without the need of any additional co-reactants.

The use of nitrogen plasma as a co-reactant has been investigated in multiple reports, in an attempt to deposit LiPON (lithium phosphorus oxynitride). Here, the nitrogen plasma showed to cross-link different adsorbed TMP molecules, through removal of their respective methoxy groups.⁴⁸ One nitrogen atom was then used to crosslink either two (-N=) or three (-N<) phosphorus atoms to form a lithium phosphorus oxynitride structure.

Nitrogen doping of phosphates was also achieved without using co-reactants, by working with “dual-source” phosphorus precursors that contain both phosphorus and nitrogen (such as DEPA or TDMAP). In the work of Shibata et al., TDMAP was for example combined with oxygen, LiO^tBu and NH₃ (in that order). In the proposed reaction scheme, the oxygen was expected to remove some of the nitrogen, although the weak nature of the reactions with oxygen limited the formation of strong P-O-P bonds and complete removal of the nitrogen terminated groups. In that way, the P-NR surface groups (with R as the carbon related ligand) that remained after the LiO^tBu step can lead to direct formation of P-N=P linked bonds in the reducing atmosphere of NH₃.

A precursor such as DEPA has shown to directly react with for example the typical tert-butoxy type precursors (either lithium- or sodium-tert-butoxide), but these reactions are very complex and not yet understood. As there also appears to be P-N-P type crosslinking (through the amine group), the complex reactions are thought to be better characterized by surface-mediated polymerisations rather than the typical ligand exchange reactions.⁵³ Note that the nature of the metal precursor ligand plays a vital role, as there showed to be clear compositional differences when using different sources for lithium. As with TMP, more de-

This is the author's peer reviewed, accepted manuscript. However, the online version of record will be different from this version once it has been copyedited and typeset.

PLEASE CITE THIS ARTICLE AS DOI: 10.1063/1.50069647

tailed research is thus needed to completely understand the complex nature of these reactions.

Plasma enhanced co-reactants for metalorganic precursor based ALD processes. For deposition processes (other than lithium phosphate) that require hydroxylation of the surface by a co-reactant, the possible use of plasma enhanced co-reactants instead of thermal reactions should be discussed as well. Recently, a detailed study was performed by Hornsveld et al., who primarily investigated the growth mechanism of TMA - O₂* - TMP - O₂* using mass spectrometry (figure 10(d)). It was found that the latter oxygen plasma step leads to the formation of gaseous CO₂, CH₃⁺ and H₂O, which indicates that the methoxy ligands of TMP are converted into -OH and/or -O species through a combustion-like reaction. The subsequent TMA pulse then results in the formation of CH₄, showing reactions with the hydroxyl ligands similar to the much discussed Al₂O₃ process. Interestingly, growth was still observed when this oxygen plasma step was removed from the deposition process, although with a lower growth rate and a high P/Al ratio of 0.8. It thus seems that TMA is able to react with the P-OCH₃ terminated surface, but this was not investigated further. The inclusion of the oxygen plasma allows for the formation of hydroxyl groups at the surface, which increase reactivity with TMA. The oxygen plasma after the TMA process step showed to remove its methyl ligands, creating -OH or -O surface species for TMP to react with. Similar to the work of Werbrouck et al. on lithium phosphate, no by-products were observed during the subsequent TMP pulse (indicating an association reaction of TMP with the hydroxylated surface rather than the typical ligand exchange often observed in ALD). This showed that the adsorbed TMP molecules remain intact during their interaction with the surface, and no reaction products in the gas phase are released. Next to this, growth was again observed without the use of an oxygen plasma step after TMA. Hornsveld et al. suggest that such reactions could take place due to a Lewis acid nature of TMP, while TMA behaves like a Lewis base allowing both molecules to participate in some association reaction. However, the P/Al ratio of a process without the oxygen plasma after the TMA process step is too low

This is the author's peer reviewed, accepted manuscript. However, the online version of record will be different from this version once it has been copyedited and typeset.

PLEASE CITE THIS ARTICLE AS DOI: 10.1063/1.50069647

and a co-reactant should thus generally be used when using such metalorganic precursors. Note that, as there is no proof of growth in a direct TMP – TMA process (only TMP – O₂* – TMA and TMP – TMA – O₂*), it cannot be fully concluded that direct reactions between TMP and TMA can lead to linear growth. These reactions could be possible (as TEP, which is fairly similar to TMP, has shown to react with TMA), but it is also possible that further growth is enabled by for example interactions of the oxygen plasma with underlying layers rather than direct reactions between TMP and TMA. In order to further understand the reactions between TMP and TMA, we performed a TMP - TMA deposition process without any additional plasma exposures using an experimental set-up similar to the one used by Dobbelaere et al.²¹ At a substrate temperature of 150°C, growth was observed at a rate of approximately 0.09 nm/cycle. The compositional ratios of the film measured using XPS (P/Al of 0.11, O/P of 12.4 and Al/O of 0.7), however, showed that the resulting film is a phosphorus doped aluminium oxide rather than a phosphate. Based on these results, it can be concluded that direct reactions between TMP and TMA can indeed result in film growth, but additional co-reactants are needed if one prefers the deposition of a metal phosphate instead of a phosphorus doped metal oxide.

In the work of Di Palma et al.⁶⁷ the reactions in the ALD process for cobalt phosphate using intermediate oxygen plasma steps was investigated using mass spectrometry as well. Starting from a surface cleaned by an oxygen plasma, the cobaltocene exposure showed no clear reaction by-product forming, pointing towards an association reaction of the complete molecule. In the subsequent oxygen plasma step, the cyclopentadienyl ligands are removed creating surface species that are reactive towards TMP vapor. This time, the TMP molecules first chemisorb on the surface (via bonding of the oxygen in P=O and the under-coordinated cobalt atoms) after which ligand exchange does occur (in contrary to the process of Hornsveld et al. and Werbrouck et al.) through elimination of a methanol molecule. The latter oxygen plasma step then allowed for a removal of the remaining TMP ligands through a combustion reaction. The difference in nature of the interaction of TMP with the surface over the course

of several different phosphates shows the complexity of the matter. While a ligand-exchange process could work in combination with one metal precursor, the entire molecule can participate in the process with a different precursor through physisorption.

These detailed studies again show that the reactions of (adsorbed) TMP and metalorganic precursors/co-reactants are very complex, are dependant on the type of metal precursor, and are generally not yet fully understood. More detailed studies like these are needed to fully understand the reactions that are taking place during each process step and further optimise the ALD processes. Nevertheless, hydroxylising the surface after either the metalorganic precursor step and/or the TMP precursor step seems to enhance the reactivity of the surface, allowing for more complete reactions to take place. It is, however, important to notice that when TMP is used as the phosphorus precursor, the connectedness of the phosphate is limited (independent of what co-reactants are used). As explained earlier, the structure of the TMP molecule will only allow you to go down to O/P atomic ratios that are expected from an orthophosphate. Other options have to be explored if one would like to shift from the deposition of an orthophosphate (by using TMP) to more connected phosphates with a lower O/P atomic ratio (such as meta- and/or polyphosphates).

Reaction mechanisms towards more connected phosphates. *Plasma polymerisation.* By turning TMP into a plasma, the bonds are locally broken and reorganised, allowing for a more interconnected phosphate. When the use of TMP plasma was first reported (for the deposition of aluminum phosphate), mass spectrometry and FTIR (figure 6(c)) were used to gain better understanding of the reactions in a $\text{TMP}^* - \text{O}_2^*$ - metal precursor process (figure 10(e)). It was found that some of the methyl ligands of TMP are transformed into hydroxyl groups during the TMP plasma process step, and different molecules could be linked to each other through P – O – P bonds. These highly reactive species could then lead to a layer of phosphorus rich phosphate esters, that are partially terminated with hydroxyl

This is the author's peer reviewed, accepted manuscript. However, the online version of record will be different from this version once it has been copyedited and typeset.

PLEASE CITE THIS ARTICLE AS DOI: 10.1063/1.50069647

groups and partially terminated with methyl ligands. As such, the plasma constitutes of a mixture of TMP plasma activated species that resemble phosphoric acid. In that way, one can use the volatility of TMP to in-situ activate it in the reactor chamber, ending up with the more favourable phosphoric acid near the substrate surface. These plasma activated species showed to polymerize on the substrate surface at a temperature below approximately 300°C, leading to very phosphorus rich and non-saturating CVD growth. At higher temperatures, the polymerisation at the surface becomes thermodynamically unfavourable (as the Gibbs free energy, determining if the polymerisation can proceed or not, becomes positive above a certain temperature²¹), and only a monolayer of phosphate esters is deposited on the surface. As some of these esters are terminated by hydroxyl groups, there are active sites for the subsequent metalorganic precursor (such as TMA) to react with. Changing the type of metalorganic precursor will then change the type of phosphate that is deposited. In that way, the plasma activation allows for a relatively easy deposition process with a high P/M ratio, a high growth per cycle and without the need for a co-reactant. Note that an additional oxygen plasma could be used after the TMP plasma pulse, which will replace the remaining methyl ligands by hydroxyl ligands, enhancing the amount of reactive sites for the subsequent metal precursor (and decreasing the amount of carbon contamination). This process mechanism is further explained for the deposition of aluminum phosphate in figure 12.

Due to the similarities between TMP and DEPA, self-saturating plasma polymerisation reactions were also observed for the latter precursor in the work of Henderick et al.^{37,55} When using an intermediate oxygen plasma, no nitrogen is present in the film and the growth per cycle and composition are close to the compositions reported by Dobbelaere et al.⁵⁴ This shows that the polymerisation of DEPA is indeed relatively similar to the polymerisation of TMP, and if the amine group would build in some nitrogen in the film, it is easily removed by the oxygen plasma. Using a nitrogen plasma instead of an oxygen plasma is thought to

This is the author's peer reviewed, accepted manuscript. However, the online version of record will be different from this version once it has been copyedited and typeset.

PLEASE CITE THIS ARTICLE AS DOI: 10.1063/1.50069647

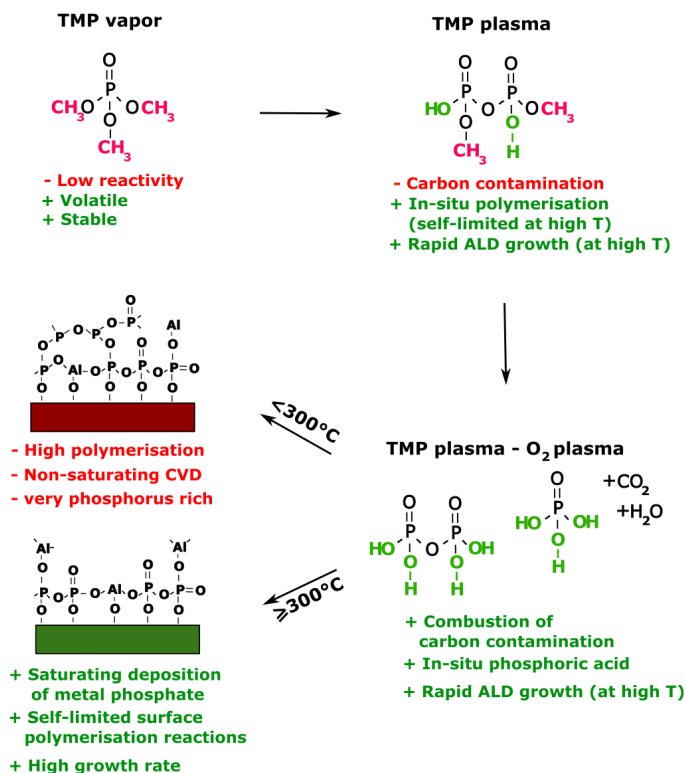


Figure 12: Plasma activation mechanism of TMP, allowing for rapid growth of metal phosphates (aluminum was used as the example here), with high P/M ratios.

remove the methoxy ligands of the adsorbed DEPA esters (as the measured carbon content was low) and link several phosphorus atoms through a P-N-P bond.

TDMAP as phosphorus source. As TDMAP does not have any pre-defined P-O bonds, it could be used to achieve a more connected phosphate when it is combined with the right co-reactant. This was clear in the work of Su et al.,¹⁹ where the TDMAP - O₂* - Mg(EtCp)₂ - H₂O process was investigated. The TDMAP molecule presumably first reacts with an -OH

This is the author's peer reviewed, accepted manuscript. However, the online version of record will be different from this version once it has been copyedited and typeset.

PLEASE CITE THIS ARTICLE AS DOI: 10.1063/1.50069647

terminated surface by the removal of one dimethylamino ligand, creating a P-O bond. For the removal of the two other dimethylamino ligands, an oxygen plasma was preferred. Co-reactants such as H_2O and O_2 were also attempted, but did not allow further growth. This is supported by the previously mentioned work of Shibata et al.,²⁸ who mentioned that only few dimethylamino ligands were replaced by hydroxyl groups by using the weakly reactive O_2 during the deposition of LiPON. If the O_2 pulse can not create enough sites that are reactive towards reaction with $\text{Mg}(\text{EtCp})_2$, growth will not be able to proceed. Oxygen plasma is expected to remove all dimethylamino sites while presumably also interlinking different phosphate groups through a P-O-P, essentially creating a surface similar to what is found after a TMP* pulse (which was explained and illustrated earlier). These surface groups are sufficiently reactive towards the subsequent $\text{Mg}(\text{EtCp})_2$ pulse, leading to the deposition of an interconnected Mg phosphate. More research needs to be done for this precursor (such as explaining its behaviour in combination with different metal precursors, mass spectrometry to confirm the reaction mechanism, etc.), but the cleaving of the dimethylamino ligands does seem to offer the possibility of interlinking different surface groups through a P-O-P bond, allowing for more connected phosphates to be deposited.

Crystallinity

As the properties of a thin film towards application can depend a lot on the crystallinity of the material, this aspect of the resulting ALD films will be briefly discussed. Apart from lithium phosphate, almost all the as-deposited ALD layers showed to be amorphous. The only report of the deposition of a crystalline (non lithium) phosphate layer is found in the work of Tiita et al.,³³ where crystalline aluminium phosphate could be deposited at 500°C using $\text{AlCl}_3 - \text{C}_4\text{H}_9\text{OH} - \text{P}_2\text{O}_5 - \text{C}_4\text{H}_9\text{OH}$. Changing the oxygen source to water again led to the deposition of an amorphous aluminium phosphate, highlighting the importance of each process parameter on the resulting structure.

For lithium phosphate, the deposition of crystalline Li_3PO_4 has been observed.^{42,51} In the

This is the author's peer reviewed, accepted manuscript. However, the online version of record will be different from this version once it has been copyedited and typeset.

PLEASE CITE THIS ARTICLE AS DOI: 10.1063/1.50069647

work of Hamalainen et al., this crystallinity was observed independently from the lithium source (LiHMDS or LiO^tBu) and over the whole temperature range that was studied (225°C-300°C for LiO^tBu and 275°C- 375°C for LiHMDS). The crystallinity showed to decrease with decreasing substrate temperature for both precursors, and was the lowest when using LiHMDS. By performing a post-deposition anneal, both films crystallised more intensely with a more pronounced grain structure. In the work of Put et al., the deposition temperature in a process using LiO^tBu was lowered to 200°C. Using this process, nearly amorphous lithium phosphate could be deposited. Increasing the temperature to 275°C resulted in the deposition of crystalline Li₃PO₄, as expected from the work of Hamalainen et al. This again shows that optimising the process parameters can play a crucial role towards the as-deposited structure and final application.

The structure of the thin film that is desired depends a lot on the application for which

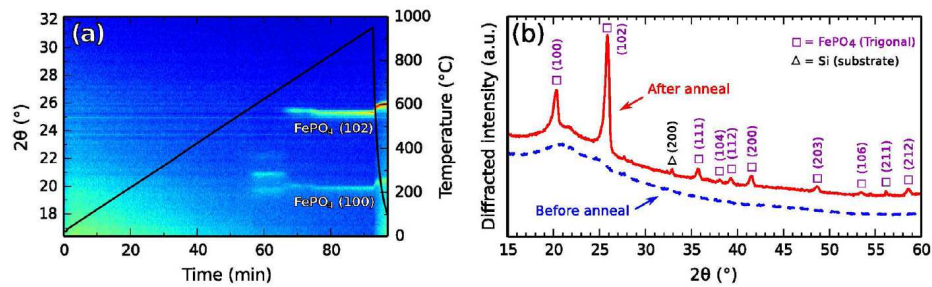


Figure 13: (a) In-situ XRD anneal of as-deposited amorphous iron phosphate deposited using TMP* - O₂* - TBF showing the formation of crystalline FePO₄ at high temperature in air. (b) ex-situ XRD to illustrate the crystallinity of the film before and after anneal. Reprinted with permission from [61]. Copyright 2016 American Chemical Society.

it will be used.² Crystalline layers could for example be desired for the specific chemical or electronic behaviour that is related to their crystalline phase. Amorphous structures on the other hand could for example be desired for their use as diffusion barriers, as grain boundaries in crystalline structures could provide leakage paths and destroy the device. Next to this, a lot of material properties could benefit from the amorphous nature of a thin film.

Focusing specifically on lithium ion batteries (or even sodium ion batteries), the transport of the ions in for example lithium⁴² or in iron phosphate⁵⁷ (and storage capacity, as will be discussed later) increases when crystallinity is lost. With these aspects in mind, it is clear that the deposition of amorphous phosphates can be of high interest for a variety of applications. Even more so, multiple reports also show that even though the as-deposited layer is amorphous, a crystalline structure can be obtained with proper post-deposition treatments.^{21,29,31,38,39,42,54,56,58,59,62,65,69,79} This is illustrated in figure 13, where amorphous iron phosphate resulting from the plasma-enhanced ALD process (TMP* - O₂* - TBF) could be transformed into crystalline FePO₄ at the correct temperature and atmosphere (in this case air). This shows that the structure of the currently available phosphates deposited through ALD is already very interesting and that, by carefully selecting the process parameters and/or post-deposition treatment, its structure could be optimised towards different applications.

From mechanisms towards applications

To obtain a phosphate of the desired stoichiometry, crystallinity or connectedness, all process parameters and precursors must be well-understood. Often, getting those perfectly right is critical for the successful practical implementation of ALD layers. The choice of precursor, and the understanding of its reaction behavior on different surfaces is essential. For example, the H-content of the films may greatly influence its properties, just as the amorphous structure, the connectedness of the phosphates, or the different crystalline phases do. Although the amount of reports on the deposition of metal phosphates is increasing, much more work is needed to obtain such an understanding. As explained earlier, the reaction mechanisms can be quite complex (especially using TMP) and are not yet well understood. A more systematic understanding on the possible reaction paths that can take place is needed, as such detailed knowledge can allow us to optimise the deposition process towards our specific needs. Not only the role of the co-reactant (e.g. how important is the choice of co-reactant

on the thin film properties) has to become more clear, the limits of certain phosphorus precursors (and how to circumvent them) have to be discussed among other things. Only by fully understanding these aspects, one is able to control the above mentioned parameters to the highest level.

The study of glassy materials has experienced enormous advances over the past years. Only now the impact of the network structure on the material properties starts to be understood. Identifying structural units is only one step towards applying knowledge from glass science in ALD research. In the previous sections, we crudely simplified the matter, as not only the composition, but also the cooling rate, pressure, and so on will influence the properties of the (generally amorphous) material. ALD-deposited materials occupy an interesting subspace of this matter, often being deposited at low pressure, below the glass transition temperature, with relatively high OH content. Hence, some experimental parameters from glass science are out of reach for us, such as the cooling rate, and the possibility to examine bulk-like samples. The deposition of phosphates with ALD is still in its infancy. Given the possible applications of 'bulk-sized' phosphates we foresee the cross-pollination between both fields to be very fruitful.⁸²⁻⁸⁴

Applications of phosphates

Although the possible applications of inorganic phosphates are wide, ALD research has mainly focused on battery and electrocatalysis applications. In the following, we will briefly sketch the concepts of these technologies, and show where ALD of phosphates has been advantageous.

Phosphate thin films for batteries

Active materials

Since the introduction of LiFePO_4 (LFP) as an active material in lithium ion batteries (LIB's), lithium containing metal phosphates have been of great interest for these applications. Starting from the basic olivine structure of the original LFP electrode, it was found that the operating potential was higher than its metal oxide counterpart (*e.g.* 2.5 V for Fe_2O_3 vs. 3.5 V for FePO_4).⁸⁵ This is observed for multiple other transition metal phosphates as well, and can be explained by the inductive effect. The presence of phosphorous in the M–O–P bond influences the covalency of the M–O bond, which effectively decreases the redox energy band and thus increases the overall cell potential. An illustration of the enhanced potential due to the presence of the phosphate polyanion (as well as the effect of different types of phosphate polyanions) can be found in figure 14. Beside this, the strong P–O bonds in the phosphate also lead to an increased thermal and structural stability, making the transition metal phosphates a safe and stable electrode material. Unlike the layered or spinel oxides, the phospho-olivine also doesn't go through a phase transformation upon full charge/discharge making them an exciting candidate as an electrode material in LIBs.^{86,87} However, the main drawback with phosphate cathodes is their low volumetric capacity (30% lower on average) to their oxide counterpart.⁸⁸ Another disadvantage is their poor electrical conductivity often leading to poor rate performance. Although crystalline materials have so far been the main focus within general battery research, the drawbacks of these materials discussed above have increased the interest to study amorphous transition metal phosphates (and LIB electrodes in general⁸⁹) as well. It was found that by losing the structural order in for example iron phosphate, more lithium ion storage sites could become available, potentially enhancing the theoretical storage capacity of the material.⁹⁰ Next to this, the reaction kinetics are also enhanced leading to improved rate performance.^{91,92} As most as-deposited metal phosphates using ALD are amorphous, this could help achieve suitable thin

film electrodes for LIB applications.

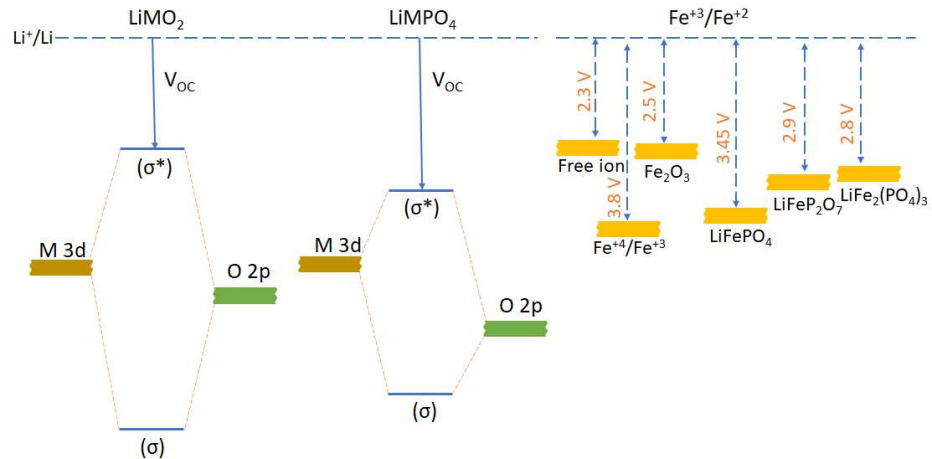


Figure 14: Energy band diagram comparison of an oxide and phosphate with respect to Li^+/Li (left). Electrode potential of $\text{Fe}^{3+}/\text{Fe}^{2+}$ process in various possible scenarios (right).

In general, the list of ALD metal phosphates used as cathode materials in LIBs is limited. Among all the materials, LiFePO_4 is the only Li-incorporated phosphate reported so far.^{56,78} LiFePO_4 is also the most studied metal phosphate in general because of low cost, iron abundance and suitable working voltage. Liu et al. successfully developed $\text{LiFePO}_4/\text{CNT}$ nanocomposites using thermal ALD by a combination of Fe_2O_3 , PO_x and Li_2O sub-cycles.⁵⁶ In an attempt to transform the as-deposited amorphous material that was obtained from this process into the most commonly studied olivine LiFePO_4 structure, the as-deposited composites were annealed at 700°C for 5h under Ar atmosphere. Mostly olivine phase LiFePO_4 was obtained after annealing along with a small amount of Fe_3P . Electrochemical characterizations of post-annealed $\text{LiFePO}_4/\text{CNT}$ materials showed excellent battery cathode performance with exceptional rate capability, power density and long term stability. The electrodes achieved as high as 150 mAh g^{-1} discharge capacity at 0.1C rate and delivered as high as 71 mAh g^{-1} capacity at 60C. Moreover, a stabilized discharge capacity of 120 mAh g^{-1} was retained throughout 2000 charge-discharge cycles. Overall the brilliant performance

This is the author's peer reviewed, accepted manuscript. However, the online version of record will be different from this version once it has been copyedited and typeset.

PLEASE CITE THIS ARTICLE AS DOI: 10.1063/1.50069647

of $\text{LiFePO}_4/\text{CNT}$ cathodes originated from uniform and conformal coating over CNTs by ALD, improved conductivity by highly crystalline LiFePO_4 and also the presence of conductive Fe_3P impurity.

In another study, Liu et al. reported the synthesis and electrochemical performance of as-grown amorphous FePO_4 coated CNT composites.⁷⁸ The CV plot of FePO_4 exhibited one pair of broad redox peaks at around 2.7 V and 3 V during discharge and charge processes respectively when cycled between 2-4 V vs Li^+/Li . The composite electrode achieved remarkable discharge capacity of 177 mAh g^{-1} at 1C in the first cycle, and exhibited capacity of 141 mAh g^{-1} after 100 battery cycles. It is to be noted that the capacity was calculated only based on FePO_4 weight, not the whole composite. In a similar kind of study by Gandrud et al., 46 nm of ALD FePO_4 was deposited on a steel substrate and showed a first cycle discharge capacity of 159 mAh g^{-1} which gradually increased and saturated to 175 mAh g^{-1} over 200 cycles.⁵⁹ The capacity then started decreasing slowly but still retained the capacity higher than the initial value even after 600 cycles. The high capacity of the two amorphous electrodes discussed above is again a clear sign of the interesting performance of non-crystalline LIB electrodes (if well optimised).

Dobbelaere et al. found that amorphous iron phosphate films deposited using the PE-ALD process needed to be cycled towards a lower potential in order to get a reasonable reversible capacity.⁶¹ The cycles following this 'activation' at low potential showed much sharper and distinguished redox peaks with lower separation voltage (0.4 V vs. 0.7 V). It was said that the initial conversion of Fe^{+3} to Fe^0 and reverting back to Fe^{+3} 'activates' the electrode for efficient intercalation/de-intercalation processes. The capacity of the redox couple was, however, still well below the theoretical capacity (see table 2), showing further optimisation would be needed to get such PE-ALD deposited thin film electrodes deposited close to 100% of theoretical capacity. A possible explanation of the lower capacity of these films with respect to the FePO_4 thin films discussed above could be the fact that different phosphate structures (for example a pyrophosphate with respect to an orthophosphate) are obtained

This is the author's peer reviewed, accepted manuscript. However, the online version of record will be different from this version once it has been copyedited and typeset.

PLEASE CITE THIS ARTICLE AS DOI: 10.1063/1.50069647

from various (PE)-ALD processes. If this is the case, it again highlights the importance of gaining more insight in the phosphate ALD processes and its resulting phosphate structure. Nevertheless, the PE-ALD iron phosphate was also deposited on a 3D micro-pillar structure, leading to a 31-fold increment in (absolute) capacity compared to planar counterpart.

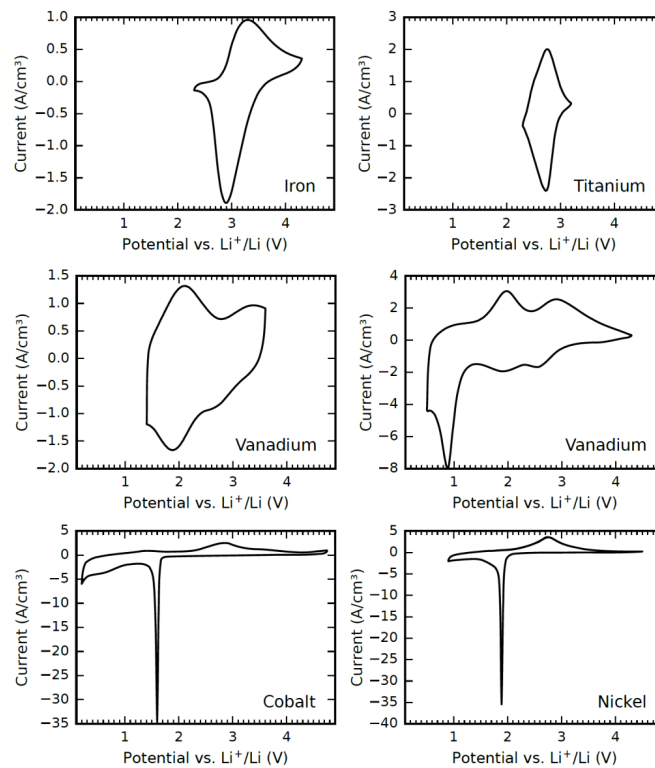


Figure 15: Summary of the electrochemical activity windows of the deposited transition metal phosphates, showing “steady-state” cyclic voltammetry patterns for iron, titanium, vanadium (two potential windows), cobalt, and nickel phosphate at 1 mV s^{-1} . Currents are normalized by volume in order to correct for varying film thicknesses. Reprinted from Thomas Dobbelaere's thesis.⁹³

Other amorphous metal phosphates like titanium and vanadium phosphates were also explored to use as electrode material for LIBs (^{54,69}). As-deposited titanium phosphate

Table 2: Overview of the potential ranges, volumetric capacities, and coulombic efficiencies measured for the as-deposited plasma enhanced-ALD phosphate films after initial lithiation. This set of data is obtained from Thomas Dobbelaere's thesis.⁹³

Transition metal	Potential range (V vs. Li ⁺ /Li)	Lithiation capacity (mAh/g)	Coulombic efficiency (%)	Theoretical capacity (mAh/g)
Iron	2.3–4.3	91	102	170
Titanium	2.3–3.2	120	99	120
	1.4–3.6	200	99	
Vanadium				197 (between 3 - 5 V vs. Li ⁺ /Li)
	0.5-4.3	620	100	
Cobalt	0.2–4.8	633	60	(170 at 4.8 V vs. Li ⁺ /Li)
Nickel	0.9–4.5	373	78	(170 at 5.1 V vs. Li ⁺ /Li)

(with approximately TiP₂O₇ stoichiometry) obtained by PEALD method showed a pair of redox peaks at around 2.7 V with a gravimetric capacity of approximately 120 mAh g⁻¹.⁵⁴ The electrochemical property of vanadium phosphate reported by Dobbelaere et al. is quite remarkable.⁶⁹ The as-deposited films contain V³⁺ which make it possible to insert/extract more than one lithium per unit. However, electrolyte decomposition at >4.5 V made the V^{4+/5+} transition not viable. Moreover, although three electrons can be transferred when the electrode cycled in the voltage range of 0.5-4 V for V³⁺ to V⁰ conversion, electrochemical performance from V^{3+/2+} is achieved from the VPO₄ + Li⁺ ↔ LiVPO₄ reaction. It does need to be noted that although the initial capacity in this extended potential range is very high, rapid capacity degradation was observed. In cycling in a smaller potential range, the overall capacity decreased but remained more stable during prolonged cycling. There also have been attempts in using the PE-ALD deposited nickel- and cobalt phosphate as LIB cathode materials, but these were only tested in a potential range below the window that is

typically proposed in literature. Although redox activity with high capacity was observed at these lower potentials, a poor coulombic efficiency and a large difference between the charge/discharge potentials has ruled out the use of these materials as an LIB electrode at the given potential ranges.

Thin film coatings

There is a general trend towards increasing the Ni-content and decreasing the Co-content in commercial NMC (LiNiMnCoO_2) cathodes. Intensive efforts are underway to achieve oxidation of Ni^{2+} and Ni^{3+} all the way to Ni^{4+} without losing oxygen from the crystal. In addition, the theoretical operating voltage of the $\text{Ni}^{2+}/\text{Ni}^{4+}$ redox pair can be as high as 4.7 V. At such high voltage, aggressive oxidation of liquid electrolyte occurs which in turn causes metal dissolution from the electrode to electrolyte followed by capacity fading.⁹⁴ To handle these issues, a lot of strategies have been adopted to functionalize the surface with various oxides, nitrides and phosphates. However, in most of the cases either they suffer from poor conductivity or non-uniformity. The conductivity issue directly hampers the lithiation-delithiation kinetics whereas non-uniformity can't provide full protection. The extreme conformality and sub-nanometer control of the ALD technique proved to be superior in functionalizing active materials and/or electrodes as a whole. There are many reports where ALD derived thin layers of oxide, nitride and phosphate protection improved the electrode performance.⁹⁵ As discussed earlier, the main advantages of phosphate thin interface layers in particular are their suitable energy band alignment, structural and (electro)chemical stability. Here, we will discuss only metal phosphate functionalization in different electrode arrangements.

Xiao et al. reported functionalization of a different, cobalt free, high-voltage LNMO ($\text{LiNi}_{0.5}\text{Mn}_{1.5}\text{O}_4$) cathode with an ALD derived ultra-thin amorphous FePO_4 layer.⁵⁷ The protective coating layer acts both as Li-diffusion facilitator during charge/discharge and buffer layer in between the LNMO cathode and liquid electrolyte. As shown in figure 16, direct electron transfer from the LUMO level of LMNO to the HOMO level of the electrolyte is

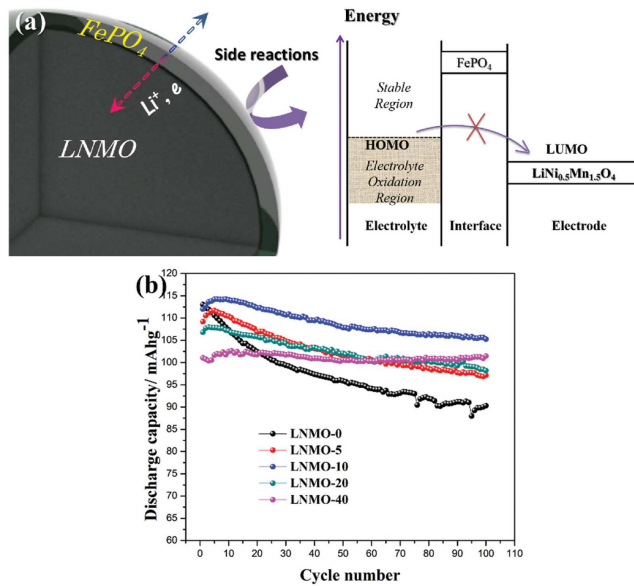


Figure 16: (a) schematic representation of functionality of FePO₄ coated LNMO particles and illustrations of energy band diagram and work functions of liquid electrolyte, FePO₄ and LNMO materials and (b) electrochemical performances of LNMO electrodes with different FePO₄ ALD cycles. reprinted from [57], Published by Wiley.

blocked due to the higher interface electrochemical potential developed by the FePO₄ layer. Another important aspect of FePO₄ is that it's an electrochemically active material and reserves some lithium inside the layer even after full charge. This small amount of lithium incorporation in FePO₄ layer assists in efficient Li-diffusion even at high current rate by providing Li⁺-ion diffusion pathways. Electrochemical performance showed that the capacity decreases with increase in FePO₄ thickness, however, 40 ALD cycle coated electrodes showed 100% capacity retention.

Another study by the same group showed the effectiveness of ALD derived AlPO₄ protection on high-energy Li-rich NMC electrode (Li_{1.2}Mn_{0.54}Co_{0.13}Ni_{0.13}O₂).³⁴ The applied buffer layer resulted in suppressing oxygen release from the crystal and also reduced electrolyte decomposition. The formation of a beneficial Li₂MnO₃ spinel like oxide phase with higher

This is the author's peer reviewed, accepted manuscript. However, the online version of record will be different from this version once it has been copyedited and typeset.

PLEASE CITE THIS ARTICLE AS DOI: 10.1063/5.0069647

ionic-conductivity during the ALD process was observed at the surface of the NMC particles. Therefore, the combination of fast ionic-transportation due to Li_2MnO_3 formation and the AlPO_4 buffer layer significantly improved the electrochemical performance of a high-energy NMC cathode. Another similar study by the same group showed the coating of the whole electrode with 10 ALD cycles AlPO_4 substantially improving the cycling stability at the expense of a slight initial capacity loss.⁹⁶ In a very recent work by Henderick et al., nitrogen-incorporation in aluminium phosphate layer (AIPON) improved the performance over the pristine material.³⁷ Even more promising was the use of titanium phosphate as an NMC coating layer, which showed to result in superior rate capabilities over the inert aluminium phosphate while still offering additional stability during cycling.⁵⁵

Table 3: Summary of ALD phosphate functionalization on different electrodes

	Active material	Coating	Thickness/ALD cycle	ALD temp.	Effects	Ref.
Cathode	$\text{LiNi}_{0.5}\text{Mn}_{1.5}\text{O}_4$	FePO_4	~2 nm, 20 cycles	300°C	Cycling stability improved, reduction in redox potential difference	57
	$\text{Li}_{1.2}\text{Mn}_{0.5}\text{Co}_{0.1}\text{Ni}_{0.1}\text{O}_2$	AlPO_4	5-40 cycles	250°C	Capacity and cycling stability improved, higher thermal stability	34
	$\text{LiNi}_{0.5}\text{Mn}_{1.5}\text{O}_4$	AlPO_4	10 cycles	250°C	Improved cycling, structural and thermal stability, suppressed Mn dissolution	96
	FePO_4	Li_3PO_4	200 cycles	250°C	Cycling stability	97
	$\text{Li}(\text{Ni}_{0.6}\text{Mn}_{0.2}\text{Co}_{0.2})\text{O}_2$	AIPON	1 cycle	325°C	cycling stability and better rate capability	37
	$\text{Li}(\text{Ni}_{0.6}\text{Mn}_{0.2}\text{Co}_{0.2})\text{O}_2$	TiPO(N)	3 cycles	300°C	Cycling stability and better rate capability	55
	$\text{LiNi}_{0.5}\text{Mn}_{1.5}\text{O}_4$	LTPO	~1nm, 10 cycles	250°C	Cycling stability and better rate capability	47
Anode	TiO_2	Li_3PO_4	~10 nm	300°C	Improvement in TiO_2 capacity	44
	MWCNT/RuO ₂	LiPON	~18 nm	250°C	Cycling and structural stability, stable SEI layer formation	50
	FeOF	LiPON	~30 nm	300°C	Extended Li-insertion before conversion process, better reversibility and capacity retention	98
	Li-terephthalate	LiPON	600 cycles	300°C	Improved rate capabilities	99
Li-metal	Li	LiPON	~10 nm	150°C	Suppressed dendrite formation	49

This is the author's peer reviewed, accepted manuscript. However, the online version of record will be different from this version once it has been copyedited and typeset.

PLEASE CITE THIS ARTICLE AS DOI: 10.1063/1.50069647

Generally, metal phosphates are mainly used for cathode protection; however, lithium phosphates (Li_3PO_4 and LiPON) can be applied on both cathodes and anodes including Li-metal protection. Liu et al. reported successful application of a 17 nm ALD LiPON layer on a 3D MWCNT/ RuO_2 electrode. The LiPON layer served two major roles there— first, it provides facile Li-diffusion pathways through the layer and keeps up the performance at high rates and secondly, it offers mechanical strength during lithiation/delithiation to help in restoring the electronic contacts among the particles. It was also found that the volume of the active layer expanded twice as much and a thicker solid electrolyte layer was formed on the CNT/ RuO_2 surface without any protection layer. In an extension of this study, the same group reported the benefits of a LiPON coating on conversion type FeOF electrodes. A very interesting observation in this particular study was found to be delaying the conversion process and prolongation of the insertion phase. Liu et al. showed an improvement in cycling stability of a 3D CNT/ FePO_4 electrode when a thin layer of Li_3PO_4 coating was employed.⁹⁷ The main advantage of Li-containing phosphate protecting coating concerns their high Li-ion conductivity through the layer while suppressing the electrolyte decomposition to a great extent. A report by Nisula et al. showed a thin LiPON layer on Li-terephthalate electrode deposited by ALD method improves the performance at high current values⁹⁹ .

Apart from protecting cathode and anode surfaces, LiPON has also been used to protect the Li-metal surface. Kozen et al. demonstrated the effectiveness of a hybrid layer consisting of an in-situ formed polymer layer which provides mechanical strength and a LiPON layer on top of the polymer layer which acts as a chemically protecting layer.⁴⁹ Such arrangement helped in suppressing the Li-dendrite formation even at high current density of 2 mA cm^{-2} over 100 plating-stripping cycles.

A novel hybrid titanium dioxide - lithium phosphate coating was also used in the work of Deng et al.,⁴⁷ where the lithium phosphate worked as an additive to the TiO_2 coating to increase the ionic conductivity of the interfacial layer. Not only did the hybrid oxide-phosphate LTPO coating protect the LMNO electrode on which it was deposited against

unwanted side-reactions, it also acted as a local network for lithium and electron transport eventually improving both cycle life and rate capability of the electrode. This shows that, next to using the phosphate itself as a coating, there are several ways to use the processes discussed in this review for enhancing the LIB electrode-electrolyte interface.

Solid electrolytes

The liquid organic electrolyte use in commercial batteries is increasingly considered to be a threat with regard to leakage, flammability, and short circuiting. In this scenario, the fabrication of all solid-state batteries enables next generation lithium-ion batteries to be safer, more portable and easily placed or patterned in small area form. The use of a non-flammable inorganic solid electrolyte not only reduces the safety concern of a storage device, it also improves the lifetime, electrochemical stability, cycling stability, and energy density. A solid electrolyte should fulfill several criteria such as high ionic and low electronic conductivity, good chemical stability and wide working electrochemical potential window. In addition to these, ALD solid electrolyte should ideally be functional in the as-grown condition, as post-deposition treatment may hamper the uniformity and conformality of the layer.

Because of their excellent structural and (electro)chemical stability, phosphates are considered to be exquisite candidates as solid electrolytes. Since their discoveries, Li_3PO_4 and LiPON have been among the most important materials in the field of solid-state batteries. They have been commonly used in commercial solid-state thin film batteries because of easy synthesis and relatively better ambient stability than other solid-state electrolytes. Among different deposition methods, reactive sputtering is the most popular technique to deposit LiPON using a Li_3PO_4 target and nitrogen as the reactive gas. However, being a physical deposition technique, sputtering is unable to deposit on high surface area substrates. Also, efficient nitrogen incorporation is still a challenge for most of the cases due to the inertness of nitrogen. Other methods like MOCVD¹⁰⁰ and e-beam evaporation¹⁰¹ were able to deposit LiPON but like most other techniques the limitation is either high temperature

This is the author's peer reviewed, accepted manuscript. However, the online version of record will be different from this version once it has been copyedited and typeset.

PLEASE CITE THIS ARTICLE AS DOI: 10.1063/5.0069647

process or limited to planar substrates. In this scenario, ALD has been proved to be a suitable technique to deposit LiPON at relatively lower temperature (100°C-300°C) and also on high surface area structures. Table 4 discusses about the reported ALD processes developed for the deposition of solid electrolytes. The highest room temperature ionic-conductivity of LiPON film reported by Kozen et al. was found to be $7.56 \times 10^{-7} \text{ S cm}^{-1}$ with 16.3% N-concentration using N_2 -plasma as the source of nitrogen, whereas the conductivity values of Li_3PO_4 vary in between 10^{-8} to $10^{-9} \text{ S cm}^{-1}$.⁴⁸ Recently, an ALD magnesium phosphate solid electrolyte with $1.7 \times 10^{-7} \text{ S cm}^{-1}$ ionic-conductivity at 500°C was reported by Su et al.¹⁹ The electrochemical performances of all-solid-state devices using ALD solid electrolyte with half cell and full cell configuration are summarised in table 5.

Table 4: Different ALD process conditions and ionic-conductivities of ALD derived metal phosphate films reported in literature

Material	Precursor	Deposition Temperature (°C)	RT conductivity (S cm^{-1})	Ref
LiPO	$\text{LiO}^t\text{Bu} + \text{TMP}$	250-325	$1.73\text{-}3.3 \times 10^{-8}$	43
	$\text{LiO}^t\text{Bu} + \text{H}_2\text{O} + \text{TMP}$	250	2.7×10^{-10}	48
	$\text{LiO}^t\text{Bu} + \text{H}_2\text{O} + \text{TMP}$	200	1.4×10^{-10}	51
LiPON	$\text{LiO}^t\text{Bu} + \text{H}_2\text{O} + \text{TMP} + \text{N}_2^*$	250	7.56×10^{-7}	48
	$\text{LiO}^t\text{Bu} + \text{H}_2\text{O} + \text{TMP} + \text{N}_2^*$	100	5×10^{-7}	51
	$\text{LiO}^t\text{Bu} + \text{DEPA}$	200-300	6.51×10^{-7}	53
	$\text{LiHMDS} + \text{DEPA}$	270-310	6.6×10^{-7}	52
	$\text{LiO}^t\text{Bu} + \text{TDMAP} + \text{NH}_3$	400-425	3.2×10^{-7}	28
MgPO_4	$\text{Mg}(\text{EtCp})_2 + \text{TDMAP}$	125-250	1.6×10^{-7} (500°C)	19

Table 5: Electrochemical performances of all solid-state cells using ALD derived Li_3PO_4 and LiPON solid-electrolytes in half-cell and full-cell configurations

Type	Battery configuration	Substrate architecture	Electrolyte thickness (nm)	Capacity/rate	Ref
Half-cell	$\text{Li}_4\text{Ti}_5\text{O}_{12}/\text{LiPON}/\text{Li}$	2D	70	$\sim 0.3 \text{ A h cm}^{-3}/5\text{C}$	⁵¹
	$\text{SnN}_x/\text{LiPON}/\text{Li}$	2D	80	$\sim 7 \mu\text{Ah cm}^{-2}/20 \mu\text{A cm}^{-2}$	¹⁰²
	$\text{LiV}_2\text{O}_5/\text{LiPON}/\text{Li}$	2D	80	$\sim 3 \mu\text{Ah cm}^{-2}/10 \mu\text{A cm}^{-2}$	¹⁰²
Full-cell	$\text{LiV}_2\text{O}_5/\text{LiPON}/\text{SnN}_x$	3D	80	$\sim 22 \mu\text{Ah cm}^{-2}/100 \mu\text{A cm}^{-2}$	¹⁰²
	$\text{LiV}_2\text{O}_5/\text{LiPON}/\text{Si}$	2D	100	$\sim 1.6 \mu\text{Ah cm}^{-2}/50 \mu\text{A cm}^{-2}$	⁵³
	$\text{LiCoO}_2/\text{LiPON}/\text{Si}$	2D	90	$\sim 16 \mu\text{Ah cm}^{-2}/300 \mu\text{A cm}^{-2}$	⁵³

Electrocatalysis

Electrocatalysis is a process that enhances the rate of an electrochemical process at the catalyst surface. Electrochemical water splitting is an important electrocatalytic process which produces O_2 and H_2 gases simultaneously. Splitting water into hydrogen and oxygen is of high interest as it could help to enable a future economy based on hydrogen fuel rather than the current fossil fuels. Water splitting is composed of two half reactions– the oxygen evolution reaction (OER) and hydrogen evolution reaction (HER). The OER process is the most demanding half reaction, involving four electron and proton transfers per molecule of O_2 produced. Usually noble metal compounds (Ru and Ir metal based) are used as catalyst for OER in acidic condition, while transition metal compounds (such as Fe, Co, Ni based oxides, chalcogenides, phosphates etc.) are being used in neutral and alkaline conditions.¹⁰³ The main problems associated with these compounds are poor conductivity, and structural and chemical instabilities during electrocatalysis. In these contexts, metal phosphates are found to be chemically more stable and to offer good structural stability.^{104,105} Next to this, an enhanced activity of the phosphates over their oxide counterparts is often found, which can be linked to the role of the phosphate group as proton acceptor, facilitating the oxidation

This is the author's peer reviewed, accepted manuscript. However, the online version of record will be different from this version once it has been copyedited and typeset.

PLEASE CITE THIS ARTICLE AS DOI: 10.1063/1.50069647

of metal atoms during proton coupled electron transfer.¹⁷ To resolve the conductivity issue, a thin metal phosphate layer on high surface area substrate could be beneficial and is therefore being actively investigated.^{105,106}

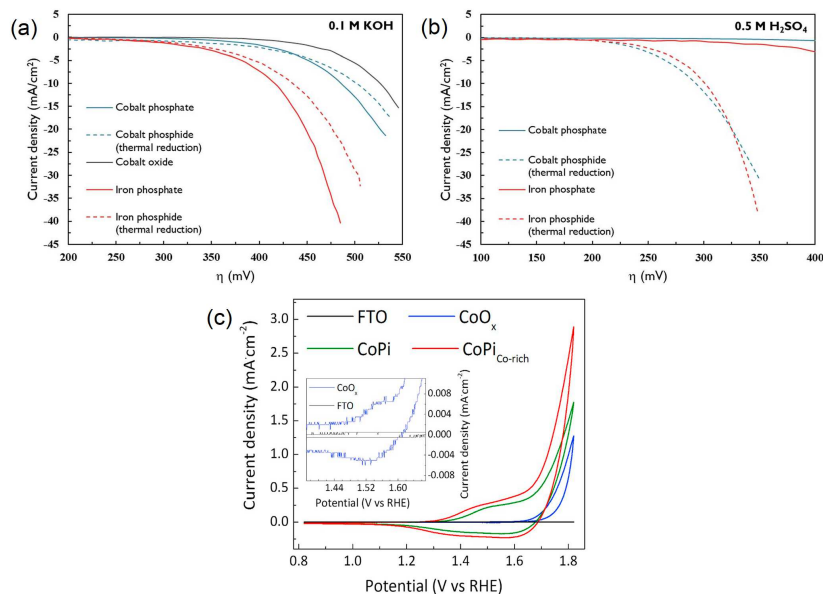


Figure 17: Current densities of catalytic reduction of different cobalt and iron compounds in (a) 0.1 M KOH and (b) 0.5 M H₂SO₄ at the rate of 1 mV S⁻¹, and cyclic voltammetry plot of Cobalt phosphate, Co-rich cobalt phosphate and reference cobalt oxide thin films after 200 cycles at 10 mV s⁻¹ scan rate; inset showing enlarged view of FTO and cobalt oxide films. Reprinted from [66,68], Published by Royal Society of Chemistry, published by Elsevier

So far, mainly Co and Fe phosphate ALD coatings have been exploited as electrocatalysts towards water splitting. A study by Rongé et al. showed the effectiveness of bi-functional phosphate/phosphide catalysts of Co and Fe produced by the combination of ALD and post-deposition treatments towards electrocatalytic water splitting.⁶⁸ During water oxidation in alkaline medium, the cobalt cations present in the pristine amorphous cobalt phosphate film oxidized, thereby likely forming a cobalt hydroxide incorporated with phosphate anions as the active material, outperforming crystalline ALD-grown Co₃O₄. Both as-grown cobalt

This is the author's peer reviewed, accepted manuscript. However, the online version of record will be different from this version once it has been copyedited and typeset.

PLEASE CITE THIS ARTICLE AS DOI: 10.1063/1.50069647

and iron phosphate were active towards hydrogen evolution in alkaline medium (Fig. 17a). During initial reducing electrochemical activation, the metals transitioned to lower oxidation states, but the phosphates were not fully converted to pure M_xP phosphides, explaining their instability in acid medium where the activated materials were found to dissolve. On the other hand, thermal post-treatment of phosphate films under reducing environment resulted in formation of M_2P , and yielded active materials for HER in acid medium (Fig. 17b). In alkaline medium, the thermally reduced material was reconverted in a phosphate material, which displayed a lower HER activity than the electrochemically activated phosphate material (Fig. 17a).

Another report by Di Palma et al. studied the electrocatalytic activity of cobalt phosphate with varying film compositions.⁶⁶ The Co-to-P ratio in the as-grown material significantly affects the catalytic performance. The current value profoundly increased from 1.77 mA cm^{-2} to 2.89 mA cm^{-2} at 1.8 V vs. RHE as shown in figure 17c when the Co/P ratio increased from 1.6 to 1.9. Prominent scopes are there for other metal phosphates and synergistic approaches as well.¹⁷

Emerging applications

Ceramic composite reinforcement. A lot of effort has been put forward to improve the mechanical and chemical properties of fiber-reinforced light weight composite materials. Reinforcements help in preventing crack propagation through the composite matrices under high stress and strain to make them more durable.¹⁰⁷ To distribute the stress throughout, there is a need of weak bonding between the fiber and composite matrices. Carbon fibers are more common to use as reinforcement with a graphitic carbon or boron nitride coating to help in forming weak bonding with the ceramic matrices.¹⁰⁸ However, both the coatings are vulnerable to moisture and oxidative environments. On the contrary, phosphate coatings are excellently oxidation resistive and showed exceptional interfacial properties like low oxygen permeability.¹⁰⁹ Knohl et al. and Militzer et al. demonstrated better stability of

This is the author's peer reviewed, accepted manuscript. However, the online version of record will be different from this version once it has been copyedited and typeset.

PLEASE CITE THIS ARTICLE AS DOI: 10.1063/1.50069647

ALD derived aluminium and titanium phosphate coating on carbon fiber bundles.^{13,35} A thin phosphate coating substantially improved thermal stability of carbon fibers towards oxidation (figure 18a) with much lesser thickness (25 nm) compared to their oxides (130 nm). *Luminescent coating.* Protective luminescent coatings have potential commercial applications. To give an example, Eu^{+3} based material is known to have the ability to convert UV radiation to red luminescence.¹¹⁰ In general, the luminescent materials are mixed with the host matrices like TiO_6^{-8} that can absorb UV light and transfer the excited electrons to Eu^{+3} band, from which the representative red emission takes place.¹¹¹ Incorporation of phosphate matrices in the crystal is believed to decrease the symmetry and emission quenching centres around Eu^{+3} which results in improving luminescent properties. Getz et al. assessed the luminescent properties of Eu-Ti binary phosphate developed by ALD method.⁷⁹ Eu-Ti-phosphate films were deposited by mixing their individual phosphates in different ratio. The as-grown samples exhibited higher degree of photobleaching ability to UV or X-rays. Annealing of these samples even further improved the luminescent properties (figure 18b), but higher temperature treatment (above 800°C) led to phase separation and thus resulting in significant shrink in emission rate.

Surface passivation of III-V semiconductors. The interest of incorporating nanostructures of III-V semiconductors in electronic and opto-electronic devices are immense. However, passivation of such nanostructures is critically important to use them in practical applications.^{112,113} Phosphorous-based III-V semiconductors such as InP, GaInP, GaAsP, etc. are usually prone to surface oxidation and effective passivation is still a challenge. Researchers have tried different materials (Al_2O_3 , SiO_2 , AlN, TiN, SiN_x , etc.)^{114,115} and deposition techniques (Wet chemical, ALD, CVD, etc.), but most of them either can not maintain the passivation or lack self-stability. Different P-rich coatings have been tried as well, including P,¹¹⁶ PO_x ,¹¹⁷ AlP_xO_y ,¹¹⁸ PO_xN_y ,¹¹⁹ etc. layers, and found to work better. The main reason of improving the passivation is due to their chemical stability and low oxygen permeability. Black et al. reported effective surface passivation of InP nanowire and planar films using

This is the author's peer reviewed, accepted manuscript. However, the online version of record will be different from this version once it has been copyedited and typeset.

PLEASE CITE THIS ARTICLE AS DOI: 10.1063/1.50069647

$\text{Al}_2\text{O}_3/\text{PO}_x$ stack layers in ALD manner at 'room temperature'.⁷¹ PO_x layer was developed using sequential dosing of TMP and O_2 -plasma at 25°C, while TMA and O_2 -plasma sequence was used for Al_2O_3 deposition at the very same temperature. The passivation was significantly capable of improving PL efficiency of InP nanowires (figure 18c). This study can also be useful for temperature sensitive substrates to be coated with phosphorous containing materials.

Biocompatible coating. The demand of biocompatible coating for the application of implants and biosensors is rapidly increasing. Calcium phosphate based coatings becoming very popular to use in such applications, among which hydroxyapatite and octacalcium phosphate, with the formula $\text{Ca}_{10}(\text{PO}_4)_6(\text{OH})_2$ and $\text{Ca}_8\text{H}_2(\text{PO}_4)_{6.5}\text{H}_2\text{O}$ are widely studied. There are several deposition techniques that have been employed to coat bioceramics onto implants, which include different physical (plasma spraying, pulsed laser, e-beam evaporation, sputtering etc.) and chemical (CVD) vapor depositions. However, poor adhesion with the implants remains one of the major drawbacks and in many cases the coating could only be realised with few specific compositions. As told previously, ALD can solve this kind of deposition problems. Putkonen et al. first reported the synthesis of biocompatible ALD derived hydroxyapatite ($\text{Ca}_{10}(\text{PO}_4)_6(\text{OH})_2$) thin films.³⁹ Biocompatibility of those thin films was evaluated using mouse MC 3T3-E1 cells (figure 18d). The observed results showed clear indication of cell attachment on the experimented substrates.

This is the author's peer reviewed, accepted manuscript. However, the online version of record will be different from this version once it has been copyedited and typeset.

PLEASE CITE THIS ARTICLE AS DOI: 10.1063/1.50069647

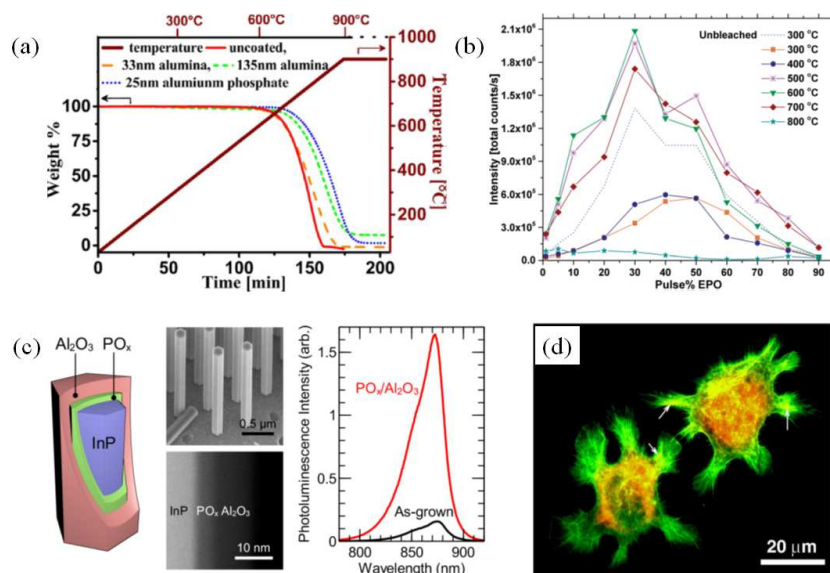


Figure 18: (a) Thermal stability analysis of uncoated, alumina and aluminum phosphate coated carbon fibers in air,³⁵ (b) Comparison of PL intensity vs. pulse percentage europium phosphate in the total supercycle of europium-titanium-phosphate at different annealing temperatures (300°C is as deposited),⁷⁹ (c) Characterization of PO_x/Al₂O₃ coated InP nanowires—schematic, SEM and TEM images, and room-temperature steady state PL spectra of coated and pristine nanowires,⁷¹ (d) The growth of MC 3T3 E1 cells for 3 h on annealed hydroxyapatite films deposited on Si substrate. Cytoskeletal actin was stained by Alexa 488 labelled phalloidin (green) and vinculin with a monoclonal antibody followed by Alexa 546 labelled anti-mouse antibody (red). The cells show clear lamellipodia and filopodia structures. Both actin and vinculin staining can be seen in these structures. Some co-localisation of these two molecules can be noticed (arrow).³⁹ Reprinted with permission from [35,79]. Copyright 2013 American Chemical Society, Published by Royal Society of Chemistry. Reprinted with permission from <https://pubs.acs.org/doi/10.1021/acs.nanolett.7b02972> by [71]. Copyright 2017 American Chemical Society. Further permission related to the material excerpted should be directed to the ACS. Reprinted with permission from [39]. Copyright 2009 Elsevier.

Conclusions and future prospects

The deposition of metal phosphates has been developed by ALD method using various phosphorous precursors and approaches. The initial idea for the deposition of metal phosphates consisted of splitting the problem in two parts: the deposition of a metal oxide using a known ALD process and a way to obtain self-limiting growth of a phosphorus oxide. In order to enable the latter, suitable phosphorus containing precursors had to be introduced. Out of several phosphorus precursors that have been reported so far, TMP has shown to be most popular due to its high vapour pressure and high stability. Nevertheless, less frequently reported precursors such as TEP or even dual-source precursors such as DEPA or TDMAP could offer some interesting properties for future processes as well. From the currently available processes, almost all of the as-grown materials have shown to be amorphous and have process temperatures ranging between 150°C-500°C depending upon the precursors involved. By changing the metallic precursor, a variety of transition metal phosphates could be deposited with a wide range of phosphorus concentrations (from phosphorus doped metal oxide to different stoichiometric phosphates by using different metal to PO_x cycle ratios). In optimising these processes, several difficulties had/have to be tackled in order to eventually obtain successful practical implementation of ALD metal phosphate layers. The low reactivity of the $-\text{OCH}_3$ ligand in TMP for example often hinders the incorporation of high phosphorus levels, making a correct choice of co-reactant in combination with a given metallic precursor crucial. A promising novel technique has already shown that by turning TMP in plasma form, *in-situ* polymerized species having reactive terminal $-\text{OH}$ groups could be integrated resulting in substantial improvements in growth rate and phosphorus content. However, more work is needed to fully optimise and understand the different reaction mechanisms in both thermal and plasma ALD-processes in order to eventually obtain full control on the final phosphate properties.

The structure of as-deposited amorphous metal phosphate is also an aspect that is still not well understood and needs our attention. The basic understanding of glass science

can help us in this prospect and here in this review we have presented few approaches to generalise the structure of such materials with respect to metal-to-phosphorus (M/P) and oxygen-to-phosphorus (O/P) ratios.

In most of the cases, ALD derived metal phosphates are used in energy storage devices till date. Starting from acting as active material to protective interface and solid electrolyte, the importance of these materials are immense in this field. Especially the olivine structure of LiFePO_4 makes it an exciting cathode material which shows higher thermal and structural stability. On the other hand, the high ionic-conductivity and simple deposition chemistry make LiPO(N) a popular choice solid electrolyte for thin film batteries. There are a number of emerging applications like electrocatalysis, luminescent displays, composite reinforcement *etc.* coming up where metal phosphates prove their strength.

Even though a reasonable number of metal phosphates have been tried till date, there are still a lot of opportunities to extend the list even further (such as nickel phosphate or even mixed transition metal phosphates). Effort should be put forward for searching for a better phosphorous precursor with high reactivity that can simplify the deposition process to a great extent. Also, the mixing of different metal phosphates (like $\text{CuTi}_2(\text{PO}_4)_3$) could have many technological importance. In another way, mixing of metal phosphates with borates or silicates can improve their physical and (electro)chemical properties appreciably. Recently, organic-inorganic hybrid materials have attracted lot of attention due to their combine advantages. In this aspect, it will be interesting to explore the deposition and properties of organo-phosphates (combination of organic part and PO_x component). In particular, this organo-phosphate could be an effective protective material for cathode and anode including Li-metal in LIBs. Perhaps they could also be used as bio-functional layer for different lab-on-a-chip devices. Apart from these, the use of phosphate coating could prove to be an useful technique in artificial bone implants and different prostheses.

This is the author's peer reviewed, accepted manuscript. However, the online version of record will be different from this version once it has been copyedited and typeset.

PLEASE CITE THIS ARTICLE AS DOI: 10.1063/1.50069647

References

- (1) George, S. M. Atomic layer deposition: an overview. *Chemical reviews* **2010**, *110*, 111–131.
- (2) Miikkulainen, V.; Leskelä, M.; Ritala, M.; Puurunen, R. L. Crystallinity of inorganic films grown by atomic layer deposition: Overview and general trends. *Journal of Applied Physics* **2013**, *113*, 2.
- (3) Puurunen, R. L. Surface chemistry of atomic layer deposition: A case study for the trimethylaluminum/water process. *Journal of applied physics* **2005**, *97*, 9.
- (4) Tynell, T.; Karppinen, M. Atomic layer deposition of ZnO: a review. *Semiconductor Science and Technology* **2014**, *29*, 043001.
- (5) Niemelä, J.-P.; Marin, G.; Karppinen, M. Titanium dioxide thin films by atomic layer deposition: a review. *Semiconductor Science and Technology* **2017**, *32*, 093005.
- (6) Hagen, D.; Pemble, M. E.; Karppinen, M. Atomic layer deposition of metals: Precursors and film growth. *Applied Physics Reviews* **2019**, *6*, 041309.
- (7) Mäntymäki, M.; Ritala, M.; Leskelä, M. Metal fluorides as lithium-ion battery materials: an atomic layer deposition perspective. *Coatings* **2018**, *8*, 277.
- (8) Dasgupta, N. P.; Meng, X.; Elam, J. W.; Martinson, A. B. Atomic layer deposition of metal sulfide materials. *Accounts of chemical research* **2015**, *48*, 341–348.
- (9) Padhi, A. K. Effect of Structure on the $\text{Fe}^{3+}/\text{Fe}^{2+}$ Redox Couple in Iron Phosphates. *Journal of The Electrochemical Society* **1997**, *144*, 1609.
- (10) Nakayama, M.; Goto, S.; Uchimoto, Y.; Wakihara, M.; Kitajima, Y. Changes in Electronic Structure between Cobalt and Oxide Ions of Lithium Cobalt Phosphate as 4.8-V Positive Electrode Material. *Chemistry of Materials* **2004**, *16*, 3399–3401.

- (11) Phuong, N. V.; Lee, K.; Chang, D.; Kim, M.; Lee, S.; Moon, S. Zinc phosphate conversion coatings on magnesium alloys: A review. *Metals and Materials International* **2013**, *19*, 273–281.
- (12) Verma, B.; Baghel, R. A Review on Luminescence properties in Eu Doped Phosphate Phosphors. *International Journal of Materials Science* **2017**, *12*, 483–489.
- (13) Militzer, C.; Buchsbaum, J.; Dzhagan, V.; Zahn, D. R. T.; Wulff, H.; Helm, C. A.; Goedel, W. A. Atomic Layer Deposition of Titanium Phosphate from Titanium Tetrachloride and Triethyl Phosphate onto Carbon Fibers. *Advanced Materials Interfaces* **2018**, *5*, 1800423.
- (14) Padhi, A. K.; Nanjundaswamy, K. S.; Goodenough, J. B. Phospho-olivines as Positive-Electrode Materials for Rechargeable Lithium Batteries. *J. Electrochem. Soc.* **1997**, *144*, 1188–1194.
- (15) Gong, Z.; Yang, Y. Recent advances in the research of polyanion-type cathode materials for Li-ion batteries. *Energy and Environmental Science* **2011**, *4*, 3223–3242.
- (16) Masquelier, C.; Croguennec, L. Polyanionic (phosphates, silicates, sulfates) frameworks as electrode materials for rechargeable Li (or Na) batteries. *Chemical Reviews* **2013**, *113*, 6552–6591.
- (17) Li, X.; Wang, J. Phosphorus-Based Electrocatalysts: Black Phosphorus, Metal Phosphides, and Phosphates. *Advanced Materials Interfaces* **2020**, *7*, 1–32.
- (18) Brow, R. K. the structure of simple phosphate glasses. *Journal of Non-Crystalline Solids* **2000**, *263*, 1–28.
- (19) Su, J.; Tsuruoka, T.; Tsujita, T.; Nishitani, Y.; Nakura, K.; Terabe, K. Atomic Layer Deposition of a Magnesium Phosphate Solid Electrolyte. *Chemistry of Materials* **2019**, *31*, 5566–5575.

This is the author's peer reviewed, accepted manuscript. However, the online version of record will be different from this version once it has been copyedited and typeset.

PLEASE CITE THIS ARTICLE AS DOI: 10.1063/1.50069647

- (20) Popović, L.; De Waal, D.; Boeyens, J. Correlation between Raman wavenumbers and P-O bond lengths in crystalline inorganic phosphates. *Journal of Raman Spectroscopy: An International Journal for Original Work in all Aspects of Raman Spectroscopy, Including Higher Order Processes, and also Brillouin and Rayleigh Scattering* **2005**, *36*, 2–11.
- (21) Dobbelaere, T.; Roy, A. K.; Vereecken, P.; Detavernier, C. Atomic Layer Deposition of Aluminum Phosphate Based on the Plasma Polymerization of Trimethyl Phosphate. *Chemistry of Materials* **2014**, *26*, 6863–6871.
- (22) Socrates, G. *Infrared and Raman characteristic group frequencies: tables and charts*; John Wiley & Sons, 2004.
- (23) Nakamoto, K. Infrared and Raman Spectra of Inorganic and Coordination Compounds. *Handbook of Vibrational Spectroscopy* **2006**,
- (24) Nieminen, M.; Niinistö, L.; Lappalainen, R. Determination of P/Al ratio in phosphorus-doped aluminium oxide thin films by XRF, RBS and FTIR. *Microchimica Acta* **1995**, *119*, 13–22.
- (25) Pallister, P. J.; Barry, S. T. Surface chemistry of group 11 atomic layer deposition precursors on silica using solid-state nuclear magnetic resonance spectroscopy. *The Journal of chemical physics* **2017**, *146*, 052812.
- (26) Young, M. J.; Yanguas-Gil, A.; Letourneau, S.; Coile, M.; Mandia, D.; Bedford, N. M.; Aoun, B.; Cavanagh, A. S.; George, S. M.; Elam, J. W. Probing the atomic-scale structure of amorphous aluminum oxide grown by atomic layer deposition. *ACS Applied Materials & Interfaces* **2020**,
- (27) Kol'tsov, S. I.; Volkova, A. N.; Aleskovskii, V. B. Preparation and investigation of the chemical composition of the products formed by successive chemisorption of titanium

This is the author's peer reviewed, accepted manuscript. However, the online version of record will be different from this version once it has been copyedited and typeset.

PLEASE CITE THIS ARTICLE AS DOI: 10.1063/1.50069647

- and phosphorus chlorides on the surface of silica gel [In Russian]. *J. Appl. Chem. USSR* **42** **1969**, 980–984.
- (28) Shibata, S. Thermal Atomic Layer Deposition of Lithium Phosphorus Oxynitride as a Thin-Film Solid Electrolyte. *Journal of The Electrochemical Society* **2016**, *163*, A2555–A2562.
- (29) Hämäläinen, J.; Holopainen, J.; Munnik, F.; Heikkilä, M.; Ritala, M.; Leskelä, M. Atomic Layer Deposition of Aluminum and Titanium Phosphates. *The Journal of Physical Chemistry C* **2012**, *116*, 5920–5925.
- (30) Wiedmann, M. K.; Jackson, D. H. K.; Pagan-Torres, Y. J.; Cho, E.; Dumesic, J. A.; Kuech, T. F. Atomic layer deposition of titanium phosphate on silica nanoparticles. *Journal of Vacuum Science & Technology A: Vacuum, Surfaces, and Films* **2012**, *30*, 01A134.
- (31) Liu, J.; Tang, Y.; Xiao, B.; Sham, T.-K.; Li, R.; Sun, X. Atomic layer deposited aluminium phosphate thin films on N-doped CNTs. *RSC Advances* **2013**, *3*, 4492.
- (32) Ishii, M.; Iwai, S.; Kawata, H.; Ueki, T.; Aoyagi, Y. Atomic layer epitaxy of ALP and its application to X-ray multilayer mirror. *Journal of crystal growth* **1997**, *180*, 15–21.
- (33) Tiitta, M.; Nykänen, E.; Soininen, P.; Niinistö, L.; Leskelä, M.; Lappalainen, R. Preparation and characterization of phosphorus-doped aluminum oxide thin films. *Materials research bulletin* **1998**, *33*, 1315–1323.
- (34) Xiao, B.; Wang, B.; Liu, J.; Kaliyappan, K.; Sun, Q.; Liu, Y.; Dadheech, G.; Balogh, M. P.; Yang, L.; Sham, T.-K.; Li, R.; Cai, M.; Sun, X. Highly stable $\text{Li}_{1.2}\text{Mn}_{0.54}\text{Co}_{0.13}\text{Ni}_{0.13}\text{O}_2$ enabled by novel atomic layer deposited AlPO_4 coating. *Nano Energy* **2017**, *34*, 120–130.

This is the author's peer reviewed, accepted manuscript. However, the online version of record will be different from this version once it has been copyedited and typeset.

PLEASE CITE THIS ARTICLE AS DOI: 10.1063/5.0069647

- (35) Knohl, S.; Roy, A. K.; Lungwitz, R.; Spange, S.; Mäder, T.; Nestler, D. J.; Wielage, B.; Schulze, S.; Hietschold, M.; Wulff, H.; Helm, C. A.; Seidel, F.; Zahn, D. R. T.; Goedel, W. A. Nonaqueous Atomic Layer Deposition of Aluminum Phosphate. *ACS Applied Materials & Interfaces* **2013**, *5*, 6161–6167.
- (36) Hornsveld, N.; Kessels, W. M. M.; Creatore, M. Atomic Layer Deposition of Aluminum Phosphate Using AlMe₃, PO(OMe)₃, and O₂ Plasma: Film Growth and Surface Reactions. *The Journal of Physical Chemistry C* **2020**, *124*, 5495–5505.
- (37) Henderick, L.; Hamed, H.; Mattelaer, F.; Minjauw, M. M.; Meersschant, J.; Dendooven, J.; Safari, M.; Vereecken, P. M.; Detavernier, C. Atomic layer deposition of nitrogen doped Al-phosphate coatings for Li-ion battery applications. *ACS Applied Materials & Interfaces* **2020**, *12*, 25949–25960, PMID: 32392406.
- (38) Brei, V.; Kaspersky, V.; Gulyanitskaya, N. Synthesis and study of boron phosphate and titanium silicate compounds on silica surface. *Reaction Kinetics and Catalysis Letters* **1993**, *50*, 415–421.
- (39) Putkonen, M.; Sajavaara, T.; Rahkila, P.; Xu, L.; Cheng, S.; Niinistö, L.; Whitlow, H. J. Atomic layer deposition and characterization of biocompatible hydroxyapatite thin films. *Thin Solid Films* **2009**, *517*, 5819–5824.
- (40) Ananda Sagari, A.; Malm, J.; Laitinen, M.; Rahkila, P.; Hongqiang, M.; Putkonen, M.; Karppinen, M.; Whitlow, H. J.; Sajavaara, T. Influence of titanium-substrate roughness on Ca–P–O thin films grown by atomic layer deposition. *Thin Solid Films* **2013**, *531*, 26–31.
- (41) Park, S. W.; Jang, D. Y.; Kim, J. W.; Shim, J. H. Fabrication of ion conductive tin oxide-phosphate amorphous thin films by atomic layer deposition. *Journal of Vacuum Science & Technology A: Vacuum, Surfaces, and Films* **2015**, *33*, 041511.

- (42) Hämäläinen, J.; Holopainen, J.; Munnik, F.; Hatanpää, T.; Heikkilä, M.; Ritala, M.; Leskelä, M. Lithium Phosphate Thin Films Grown by Atomic Layer Deposition. *Journal of The Electrochemical Society* **2012**, *159*, A259–A263.
- (43) Wang, B.; Liu, J.; Sun, Q.; Li, R.; Sham, T.-K.; Sun, X. Atomic layer deposition of lithium phosphates as solid-state electrolytes for all-solid-state microbatteries. *Nanotechnology* **2014**, *25*, 504007.
- (44) Létiche, M.; Eustache, E.; Freixas, J.; Demortière, A.; Andrade, V. D.; Morgenroth, L.; Tilmant, P.; Vaurette, F.; Troadec, D.; Roussel, P.; Brousse, T.; Lethien, C. Atomic Layer Deposition of Functional Layers for on Chip 3D Li-Ion All Solid State Micro-battery. *Advanced Energy Materials* **2016**, *7*, 1601402.
- (45) Werbrouck, A.; Mattelaer, F.; Minjauw, M.; Nisula, M.; Julin, J.; Munnik, F.; Dendooven, J.; Detavernier, C. Reaction Pathways for Atomic Layer Deposition with Lithium Hexamethyl Disilazide, Trimethyl Phosphate, and Oxygen Plasma. *The Journal of Physical Chemistry C* **2020**,
- (46) Wang, B.; Liu, J.; Sun, Q.; Xiao, B.; Li, R.; Sham, T.-K.; Sun, X. Titanium Dioxide/Lithium Phosphate Nanocomposite Derived from Atomic Layer Deposition as a High-Performance Anode for Lithium Ion Batteries. *Advanced Materials Interfaces* **2016**, *3*, 1600369.
- (47) Deng, S. et al. Manipulation of an ionic and electronic conductive interface for highly-stable high-voltage cathodes. *Nano Energy* **2019**, *65*, 103988.
- (48) Kozen, A. C.; Pearse, A. J.; Lin, C.-F.; Noked, M.; Rubloff, G. W. Atomic Layer Deposition of the Solid Electrolyte LiPON. *Chemistry of Materials* **2015**, *27*, 5324–5331.
- (49) Kozen, A. C.; Lin, C.-F.; Zhao, O.; Lee, S. B.; Rubloff, G. W.; Noked, M. Stabilization

This is the author's peer reviewed, accepted manuscript. However, the online version of record will be different from this version once it has been copyedited and typeset.

PLEASE CITE THIS ARTICLE AS DOI: 10.1063/5.0069647

- of Lithium Metal Anodes by Hybrid Artificial Solid Electrolyte Interphase. *Chemistry of Materials* **2017**, *29*, 6298–6307.
- (50) Lin, C.-F.; Noked, M.; Kozen, A. C.; Liu, C.; Zhao, O.; Gregorczyk, K.; Hu, L.; Lee, S. B.; Rubloff, G. W. Solid Electrolyte Lithium Phosphous Oxynitride as a Protective Nanocladding Layer for 3D High-Capacity Conversion Electrodes. *ACS Nano* **2016**, *10*, 2693–2701.
- (51) Put, B.; Mees, M. J.; Hornsveld, N.; Hollevoet, S.; Sepúlveda, A.; Vereecken, P. M.; Kessels, W. M. M.; Creatore, M. Plasma-Assisted ALD of LiPO(N) for Solid State Batteries. *Journal of The Electrochemical Society* **2019**, *166*, A1239–A1242.
- (52) Nisula, M.; Shindo, Y.; Koga, H.; Karppinen, M. Atomic Layer Deposition of Lithium Phosphorus Oxynitride. *Chemistry of Materials* **2015**, *27*, 6987–6993.
- (53) Pearse, A. J.; Schmitt, T. E.; Fuller, E. J.; El-Gabaly, F.; Lin, C.-F.; Gerasopoulos, K.; Kozen, A. C.; Talin, A. A.; Rubloff, G.; Gregorczyk, K. E. Nanoscale Solid State Batteries Enabled by Thermal Atomic Layer Deposition of a Lithium Polyphosphazene Solid State Electrolyte. *Chemistry of Materials* **2017**, *29*, 3740–3753.
- (54) Dobbelaere, T.; Mattelaer, F.; Roy, A. K.; Vereecken, P.; Detavernier, C. Plasma-enhanced atomic layer deposition of titanium phosphate as an electrode for lithium-ion batteries. *Journal of Materials Chemistry A* **2017**, *5*, 330–338.
- (55) Henderick, L.; Hamed, H.; Mattelaer, F.; Minjauw, M.; Nisula, M.; Meersschant, J.; Dendooven, J.; Safari, M.; Vereecken, P.; Detavernier, C. Plasma enhanced atomic layer deposition of a (nitrogen doped) Ti phosphate coating for improved energy storage in Li-ion batteries. *Journal of Power Sources* **2021**, *497*, 229866.
- (56) Liu, J.; Banis, M. N.; Sun, Q.; Lushington, A.; Li, R.; Sham, T.-K.; Sun, X. Rational Design of Atomic-Layer-Deposited LiFePO₄ as a High-Performance Cathode for Lithium-Ion Batteries. *Advanced Materials* **2014**, *26*, 6472–6477.

- (57) Xiao, B.; Liu, J.; Sun, Q.; Wang, B.; Banis, M. N.; Zhao, D.; Wang, Z.; Li, R.; Cui, X.; Sham, T.-K.; Sun, X. Unravelling the Role of Electrochemically Active FePO_4 Coating by Atomic Layer Deposition for Increased High-Voltage Stability of $\text{LiNi}_{0.5}\text{Mn}_{1.5}\text{O}_4$ Cathode Material. *Advanced Science* **2015**, *2*, 1500022.
- (58) Chernyaeva, O.; Kyashkin, V.; Ivleva, A.; Yrova, V.; Solovyova, E. The influence of process conditions on the phase composition of the LiFePO_4 film obtained by the atomic layer method. *Polyhedron* **2019**, *157*, 297–300.
- (59) Gandrud, K. B.; Pettersen, A.; Nilsen, O.; Fjellvåg, H. High-performing iron phosphate for enhanced lithium ion solid state batteries as grown by atomic layer deposition. *J. Mater. Chem. A* **2013**, *1*, 9054–9059.
- (60) Brennhagen, A.; Kvamme, K. B.; Sverdlilje, K. S.; Nilsen, O. High power iron phosphate cathodes by atomic layer deposition. *Solid State Ionics* **2020**, *353*, 115377.
- (61) Dobbelaere, T.; Mattelaer, F.; Dendooven, J.; Vereecken, P.; Detavernier, C. Plasma-Enhanced Atomic Layer Deposition of Iron Phosphate as a Positive Electrode for 3D Lithium-Ion Microbatteries. *Chemistry of Materials* **2016**, *28*, 3435–3445.
- (62) Sønsteby, H. H.; Østreng, E.; Fjellvåg, H.; Nilsen, O. Atomic Layer Deposition of LaPO_4 and Ca:LaPO_4 . *Chemical Vapor Deposition* **2014**, *20*, 269–273.
- (63) Yuan, H.; Luo, B.; Campbell, S. A.; Gladfelter, W. L. Atomic Layer Deposition of p-Type Phosphorus-Doped Zinc Oxide Films Using Diethylzinc, Ozone and Trimethylphosphite. *Electrochemical and Solid-State Letters* **2011**, *14*, H181.
- (64) Tynell, T.; Okazaki, R.; Terasaki, I.; Yamauchi, H.; Karppinen, M. Electron doping of ALD-grown ZnO thin films through Al and P substitutions. *Journal of Materials Science* **2012**, *48*, 2806–2811.

This is the author's peer reviewed, accepted manuscript. However, the online version of record will be different from this version once it has been copyedited and typeset.

PLEASE CITE THIS ARTICLE AS DOI: 10.1063/5.0069647

- (65) Dobbelaere, T.; Minjauw, M.; Ahmad, T.; Vereecken, P.; Detavernier, C. Plasma-enhanced atomic layer deposition of zinc phosphate. *Journal of Non-Crystalline Solids* **2016**, *444*, 43–48.
- (66) Palma, V. D.; Zafeiropoulos, G.; Goldsweer, T.; Kessels, W.; van de Sanden, M.; Creatore, M.; Tsampas, M. Atomic layer deposition of cobalt phosphate thin films for the oxygen evolution reaction. *Electrochemistry Communications* **2019**, *98*, 73–77.
- (67) Di Palma, V.; Knoop, H. C.; Kessels, W. M.; Creatore, M. Atomic layer deposition of cobalt phosphate from cobaltocene, trimethylphosphate, and O₂ plasma. *Journal of Vacuum Science & Technology A: Vacuum, Surfaces, and Films* **2020**, *38*, 022416.
- (68) Rongé, J.; Dobbelaere, T.; Henderick, L.; Minjauw, M. M.; Sree, S. P.; Dendooven, J.; Martens, J. A.; Detavernier, C. Bifunctional earth-abundant phosphate/phosphide catalysts prepared via atomic layer deposition for electrocatalytic water splitting. *Nanoscale Advances* **2019**, *1*, 4166–4172.
- (69) Dobbelaere, T.; Mattelaer, F.; Vereecken, P. M.; Detavernier, C. Plasma-enhanced atomic layer deposition of vanadium phosphate as a lithium-ion battery electrode material. *Journal of Vacuum Science & Technology A: Vacuum, Surfaces, and Films* **2017**, *35*, 041513.
- (70) Nuwayhid, R. B.; Jarry, A.; Rubloff, G. W.; Gregorczyk, K. E. Atomic Layer Deposition of Sodium Phosphorus Oxynitride: A Conformal Solid-State Sodium-Ion Conductor. *ACS Applied Materials & Interfaces* **2020**, *12*, 21641–21650.
- (71) Black, L. E.; Cavalli, A.; Verheijen, M. A.; Haverkort, J. E. M.; Bakkers, E. P. A. M.; Kessels, W. M. M. Effective Surface Passivation of InP Nanowires by Atomic-Layer-Deposited Al₂O₃ with PO_x Interlayer. *Nano Letters* **2017**, *17*, 6287–6294.
- (72) Knemeyer, K.; Hermida, M. P.; Ingale, P.; Schmidt, J.; Kröhnert, J.; d'Alnoncourt, R. N.; Driess, M.; Rosowski, F. Mechanistic Studies of Atomic Layer

This is the author's peer reviewed, accepted manuscript. However, the online version of record will be different from this version once it has been copyedited and typeset.

PLEASE CITE THIS ARTICLE AS DOI: 10.1063/1.50069647

- Deposition on Oxidation Catalysts- AlO_x and PO_x Deposition. *Physical Chemistry Chemical Physics* **2020**,
- (73) Kalkofen, B.; Ahmed, B.; Beljakowa, S.; Lisker, M.; Kim, Y.; Butte, E. P. Atomic layer deposition of phosphorus oxide films as solid sources for doping of semiconductor structures. 2018 IEEE 18th International Conference on Nanotechnology (IEEE-NANO). 2018; pp 1–4.
- (74) Malygin, A.; Koltsov, S.; Aleskovskii, V. Chemical Composition of Chromium and Phosphorus-Containing Silica, Synthesized by Molecular Stratification Method. *ZHURNAL OBSHCHEI KHIMII* **1980**, *50*, 2633–2636.
- (75) Nilsen, O.; Miikkulainen, V.; Gandrud, K. B.; Østreng, E.; Ruud, A.; Fjellvåg, H. Atomic layer deposition of functional films for Li-ion microbatteries. *physica status solidi (a)* **2014**, *211*, 357–367.
- (76) Lacivita, V.; Westover, A. S.; Kercher, A.; Phillip, N. D.; Yang, G.; Veith, G.; Ceder, G.; Dudney, N. J. Resolving the amorphous structure of lithium phosphorus oxynitride (Lipon). *Journal of the American Chemical Society* **2018**, *140*, 11029–11038.
- (77) Saulys, D.; Joshkin, V.; Khoudiakov, M.; Kuech, T.; Ellis, A.; Oktyabrsky, S.; McCaughan, L. An examination of the surface decomposition chemistry of lithium niobate precursors under high vacuum conditions. *Journal of crystal growth* **2000**, *217*, 287–301.
- (78) Liu, J.; Xiao, B.; Banis, M. N.; Li, R.; Sham, T.-K.; Sun, X. Atomic layer deposition of amorphous iron phosphates on carbon nanotubes as cathode materials for lithium-ion batteries. *Electrochimica Acta* **2015**, *162*, 275–281.
- (79) Getz, M. N.; Hansen, P.-A.; Fjellvåg, H.; Nilsen, O. Luminescent properties of eu-

This is the author's peer reviewed, accepted manuscript. However, the online version of record will be different from this version once it has been copyedited and typeset.

PLEASE CITE THIS ARTICLE AS DOI: 10.1063/1.50069647

- ropium titanium phosphate thin films deposited by atomic layer deposition. *RSC Advances* **2017**, *7*, 8051–8059.
- (80) Diskus, M.; Nilsen, O.; Fjellvåg, H. Thin films of cobalt oxide deposited on high aspect ratio supports by atomic layer deposition. *Chemical Vapor Deposition* **2011**, *17*, 135–140.
- (81) Kvamme, K. B. Phosphites in Atomic Layer Deposition Synthesis and Characterisation Using Unconventional Phosphorous Precursors. M.Sc. thesis, 2016.
- (82) Hofmann, P.; Walther, F.; Rohnke, M.; Sann, J.; Zeier, W. G.; Janek, J. LATP and LiCoPO₄ thin film preparation—Illustrating interfacial issues on the way to all-phosphate SSBs. *Solid State Ionics* **2019**, *342*, 115054.
- (83) Sales, B. C. Phosphate glasses. *MRS Bulletin* **1987**, *12*, 32–35.
- (84) Musgraves, J. D.; Hu, J.; Calvez, L. *Springer Handbook of Glass*; Springer Nature, 2019.
- (85) Thackeray, M. M.; David, W. I. F.; Goodenough, J. B. Structural characterization of the lithiated iron oxides Li_xFe₃O₄ and Li_xFe₂O₃ (0 < x < 2). *Materials Research Bulletin* **1982**, *17*, 785–793.
- (86) Jing Xu, Feng Lin, M. M. D.; Tong, W. A review of Ni-based layered oxides for rechargeable Li-ion batteries. *Journal of Materials Chemistry A* **2017**, *5*, 874–901.
- (87) Zaghbi, K.; Mauger, A.; Julien, C. M. In *Rechargeable Batteries: Materials, Technologies and New Trends*; Zhang, Z., Zhang, S. S., Eds.; Springer International Publishing: Cham, 2015; pp 25–65.
- (88) Hautier, G.; Jain, A.; Ong, S. P.; Kang, B.; Moore, C.; Doe, R.; Ceder, G. Phosphates as lithium-ion battery cathodes: An evaluation based on high-throughput ab initio calculations. *Chemistry of Materials* **2011**, *23*, 3495–3508.

This is the author's peer reviewed, accepted manuscript. However, the online version of record will be different from this version once it has been copyedited and typeset.

PLEASE CITE THIS ARTICLE AS DOI: 10.1063/1.50069647

- (89) Fang, H.-T.; Liu, M.; Wang, D.-W.; Sun, T.; Guan, D.-S.; Li, F.; Zhou, J.; Sham, T.-K.; Cheng, H.-M. Comparison of the rate capability of nanostructured amorphous and anatase TiO₂ for lithium insertion using anodic TiO₂ nanotube arrays. *Nanotechnology* **2009**, *20*, 225701.
- (90) Gerbaldi, C.; Meligrana, G.; Bodoardo, S.; Tuel, A.; Penazzi, N. FePO₄ nanoparticles supported on mesoporous SBA-15: Interesting cathode materials for Li-ion cells. *Journal of power sources* **2007**, *174*, 501–507.
- (91) Wei, Z.; Wang, D.; Yang, X.; Wang, C.; Chen, G.; Du, F. From Crystalline to Amorphous: An Effective Avenue to Engineer High-Performance Electrode Materials for Sodium-Ion Batteries. *Advanced Materials Interfaces* **2018**, *5*, 1800639.
- (92) Liu, C.; Neale, Z. G.; Cao, G. Understanding electrochemical potentials of cathode materials in rechargeable batteries. *Materials Today* **2016**, *19*, 109–123.
- (93) Dobbelaere, T. Plasma-enhanced atomic layer deposition of transition metal phosphates. Ph.D. thesis, 2017.
- (94) Manthiram, A. A reflection on lithium-ion battery cathode chemistry. *Nature Communications* **2020**, *11*, 1–9.
- (95) Guan, C.; Wang, J. Recent Development of Advanced Electrode Materials by Atomic Layer Deposition for Electrochemical Energy Storage. *Advanced Science* **2016**, *3*, 1–23.
- (96) Deng, S.; Xiao, B.; Wang, B.; Li, X.; Kaliyappan, K.; Zhao, Y.; Lushington, A.; Li, R.; Sham, T. K.; Wang, H.; Sun, X. New insight into atomic-scale engineering of electrode surface for long-life and safe high voltage lithium ion cathodes. *Nano Energy* **2017**, *38*, 19–27.

This is the author's peer reviewed, accepted manuscript. However, the online version of record will be different from this version once it has been copyedited and typeset.

PLEASE CITE THIS ARTICLE AS DOI: 10.1063/1.50069647

- (97) Liu, J.; Wang, B.; Sun, Q.; Li, R.; Sham, T. K.; Sun, X. Atomic Layer Deposition of Hierarchical CNTs@FePO₄ Architecture as a 3D Electrode for Lithium-Ion and Sodium-Ion Batteries. *Advanced Materials Interfaces* **2016**, *3*, 1600468 1–7.
- (98) Lin, C. F.; Fan, X.; Pearse, A.; Liou, S. C.; Gregorczyk, K.; Leskes, M.; Wang, C.; Lee, S. B.; Rubloff, G. W.; Noked, M. Highly Reversible Conversion-Type FeOF Composite Electrode with Extended Lithium Insertion by Atomic Layer Deposition LiPON Protection. *Chemistry of Materials* **2017**, *29*, 8780–8791.
- (99) Nisula, M.; Karppinen, M. Atomic/Molecular Layer Deposition of Lithium Terephthalate Thin Films as High Rate Capability Li-Ion Battery Anodes. *Nano Letters* **2016**, *16*, 1276–1281.
- (100) Fujibayashi, T.; Kubota, Y.; Iwabuchi, K.; Yoshii, N. Highly conformal and high-ionic conductivity thin-film electrolyte for 3D-structured micro batteries: Characterization of LiPON film deposited by MOCVD method. *AIP Advances* **2017**, *7*.
- (101) Liu, W.-Y.; Fu, Z.-W.; Li, C.-L.; Qin, Q.-Z. Lithium Phosphorus Oxynitride Thin Film Fabricated by a Nitrogen Plasma-Assisted Deposition of E-beam Reaction Evaporation. *Electrochemical and Solid-State Letters* **2004**, *7*, J36.
- (102) Pearse, A.; Schmitt, T.; Sahadeo, E.; Stewart, D. M.; Kozen, A.; Gerasopoulos, K.; Talin, A. A.; Lee, S. B.; Rubloff, G. W.; Gregorczyk, K. E. Three-Dimensional Solid-State Lithium-Ion Batteries Fabricated by Conformal Vapor-Phase Chemistry. *ACS Nano* **2018**, *12*, 4286–4294.
- (103) McCrory, C. C.; Jung, S.; Peters, J. C.; Jaramillo, T. F. Benchmarking heterogeneous electrocatalysts for the oxygen evolution reaction. *Journal of the American Chemical Society* **2013**, *135*, 16977–16987.
- (104) Guo, R.; Lai, X.; Huang, J.; Du, X.; Yan, Y.; Sun, Y.; Zou, G.; Xiong, J. Phosphate-

This is the author's peer reviewed, accepted manuscript. However, the online version of record will be different from this version once it has been copyedited and typeset.

PLEASE CITE THIS ARTICLE AS DOI: 10.1063/1.50069647

- based electrocatalysts for water splitting: recent progress. *ChemElectroChem* **2018**, *5*, 3822–3834.
- (105) Zhao, H.; Yuan, Z.-Y. Insights into Transition Metal Phosphate Materials for Efficient Electrocatalysis. *ChemCatChem* **2020**,
- (106) Yuan, C.-Z.; Jiang, Y.-F.; Wang, Z.; Xie, X.; Yang, Z.-K.; Yousaf, A. B.; Xu, A.-W. Cobalt phosphate nanoparticles decorated with nitrogen-doped carbon layers as highly active and stable electrocatalysts for the oxygen evolution reaction. *Journal of Materials Chemistry A* **2016**, *4*, 8155–8160.
- (107) Naslain, R. R. The design of the fibre-matrix interfacial zone in ceramic matrix composites. *Composites Part A: Applied Science and Manufacturing* **1998**, *29*, 1145 – 1155.
- (108) Naslain, R.; Dugne, O.; Guette, A.; Sevely, J.; Brosse, C. R.; Rocher, J.-P.; Cotteret, J. Boron Nitride Interphase in Ceramic-Matrix Composites. *Journal of the American Ceramic Society* **1991**, *74*, 2482–2488.
- (109) Morgan, P. E. D.; Marshall, D. B. Ceramic Composites of Monazite and Alumina. *Journal of the American Ceramic Society* **1995**, *78*, 1553–1563.
- (110) Chen, J.-Y.; Huang, C.; Hung, W.; Sun, K.; Chen, T. Efficiency improvement of Si solar cells using metal-enhanced nanophosphor fluorescence. *Solar Energy Materials and Solar Cells* **2014**, *120*, 168 – 174.
- (111) Hansen, P.-A.; Fjellvåg, H.; Finstad, T. G.; Nilsen, O. Luminescent Properties of Multilayered Eu₂O₃ and TiO₂ Grown by Atomic Layer Deposition**. *Chemical Vapor Deposition* **2014**, *20*, 274–281.
- (112) Robertson, J.; Guo, Y.; Lin, L. Defect state passivation at III-V oxide interfaces for

- complementary metal–oxide–semiconductor devices. *Journal of Applied Physics* **2015**, *117*, 112806.
- (113) Houssa, M.; Chagarov, E.; Kummel, A. Surface Defects and Passivation of Ge and III–V Interfaces. *MRS Bulletin* **2009**, *34*, 504–513.
- (114) Dhaka, V.; Perros, A.; Naureen, S.; Shahid, N.; Jiang, H.; Kakko, J.-P.; Haggren, T.; Kauppinen, E.; Srinivasan, A.; Lipsanen, H. Protective capping and surface passivation of III-V nanowires by atomic layer deposition. *AIP Advances* **2016**, *6*, 015016.
- (115) Sautreuil, B.; Viktorovitch, P.; Blanchet, R. Evidence for interfacial defects in metal-insulator-InP structures induced by the insulator deposition. *Journal of Applied Physics* **1985**, *57*, 2322–2324.
- (116) Schachter, R.; Olego, D. J.; Baumann, J. A.; Bunz, L. A.; Raccah, P. M.; Spicer, W. E. Interfacial properties of InP and phosphorus deposited at low temperature. *Applied Physics Letters* **1985**, *47*, 272–274.
- (117) Pande, K. P.; Gutierrez, D. Channel mobility enhancement in InP metal-insulator-semiconductor field-effect transistors. *Applied Physics Letters* **1985**, *46*, 416–418.
- (118) Meiners, L. Electrical properties of Al₂O₃ and AlP_xO_y dielectric layers on InP. *Thin Solid Films* **1984**, *113*, 85 – 92.
- (119) Hbib, H.; Bonnaud, O.; Gauneau, M.; Hamedi, L.; Marchand, R.; Quemerais, A. Characterization of phosphorus oxinitride (PON) gate insulators for InP metal-insulator-semiconductor devices. *Thin Solid Films* **1997**, *310*, 1 – 7.

Acknowledgements

The authors are grateful for financial support to FWO-Vlaanderen and the Special Research Fund BOF of Ghent University (GOA project, Grant No. 01G01019, and SBO XL-Lion,

This is the author's peer reviewed, accepted manuscript. However, the online version of record will be different from this version once it has been copyedited and typeset.

PLEASE CITE THIS ARTICLE AS DOI: 10.1063/5.0069647

S005017N). J.D. acknowledges FWO-Vlaanderen for a post-doctoral fellowship.

Author declarations

Conflicts of interest

The authors have no conflicts to disclose.

Data availability statement

The data that support the findings of this study are available from the corresponding author upon reasonable request.